# Anisotropic Structure and Dynamics of Water under Static Electric Fields

Mahdi Shafiei[1], Michael von Domaros[2], Dusan Bratko[1], and Alenka Luzar[1]

[1]Department of Chemistry, Virginia Commonwealth University, Richmond, Virginia 23284-2006, United States.
[2] Department of Chemistry, University of California, Irvine, Irvine, California 92697, United States

Abstract

We study the structure and dynamics of water subject to a range of static external electric fields, using molecular dynamics simulations. In particular, we monitor the changes in hydrogen bond kinetics, reorientation dynamics, and translational motions of water molecules. We find that water molecules translate and rotate slower in electric fields, because the tendency to reinstate the aligned orientation reduces the probability of finding a new hydrogen bond partner and hence increases the probability of reforming already ruptured bonds. Furthermore, dipolar alignment of water molecules with the field results in structural and dynamic anisotropies even though the angularly averaged metrics indicate only minor structural changes. Through comparison of selected nonpolarizable and polarizable water models, we find that the electric field effects are stronger in polarizable water models, where field-enhanced dipole moments and thus more stable hydrogen bonds lead to slower switching of hydrogen bond partners and reduced translational mobility, compared to a nonpolarizable water model.

## 1. INTRODUCTION

Water is a polar solvent possessing relatively large electric dipole and quadrupole moments[1] that interact strongly with external electric fields (E-fields). Their imposition can induce significant changes in fundamental water properties,[2] notably in density,[3-5] diffusion,[6] and viscosity,[7,8] both in the bulk[9] and in confinement.[10] Not surprisingly, field related phenomena have been the subject of many previous experimental and computational studies and various applications have emerged (see ref.[11] for a recent review).

Much of the previous work has focused on the structure of water subject to E-fields. Sutmann[12] has reported that water molecules mostly line up with the field of $\sim 0.1 \mathrm{V\AA^{-1}}$, while an unrealistic strength of $3.0\ \mathrm{V\AA^{-1}}$ would be needed to convert the liquid to a highly ordered ice. Saitta *et al.*[13] have performed ab initio simulations on bulk water and show that its structure is only slightly enhanced with characteristic order parameters changed by less than 2 % under electric fields of up to $0.2\ \mathrm{V\AA^{-1}}$. Vegiri[14,15] observes a significant shift of the peak of the radial distribution function (RDF) of water at $250$ K under unphysical E-fields of $0.4\ \mathrm{V\AA^{-1}}$ or stronger.

Various works have also been performed from a thermodynamic perspective. Amadei *et al.*[16] have developed a quasi-Gaussian entropy (QGE) theory for the thermodynamics of dielectric fluids as a function of temperature and the strength of the E-field and Aragones *et al.*[17] have calculated the effect of the strength of the static E-field on the phase diagram of water.

While the primary effect of static external electric fields on water dipolar alignment is easy to conceptualize, it competes with the local directional preferences of water molecules engaged in up to four stable hydrogen bonds.[18-24] As a consequence, understanding the precise impact of electric fields on water reorientation and hydrogen bond (HB) dynamics remains an unresolved problem, even in bulk water. Slower hydrogen bond breaking and reforming[2,18] has been conjectured to be the cause of decelerated diffusion in field-imposed water, but systematic analyses are lacking.

Here, we address such questions by a careful structure analysis and by studying the relation between HB kinetics[25-33] and its coupling to diffusion,[25,33-42] subject to static external electric fields. Our analysis builds on/extends the established hydrogen bond kinetics phenomenology by Luzar and Chandler.[25] We compare different water models and investigate a range of static electric fields with strengths between $0.01\ \mathrm{V\AA^{-1}}$, where E-field alignment becomes detectable,[3] and $0.2\ \mathrm{V\AA^{-1}}$, avoiding the proximity of the dissociation threshold of $\sim 0.3\ \mathrm{V\AA^{-1}}$.[13,43] Our simulated fields extend well above the commonly accepted dielectric strength of $\sim 7 \cdot 10^{-3}$ $\mathrm{V\AA^{-1}}$ in bulk water, however, a significantly higher threshold strength is indicated by experiments in μm films of deionized water when current is prevented by adequate insulation[44]. Static fields up to an order of magnitude above the dielectric strength of the bulk water are also known to pervade water in ion channels[45] and next to ionic colloids[46] or liquid crystals[47]. Local field amplitudes in excess of ~2 $\mathrm{V\AA^{-1}}$, accompanying perpetual structural fluctuations, have been manifested by Raman spectroscopy[48] and direct molecular simulations in liquid water[48,49].

## 2. MODELS AND METHODS

### 2.1. Computational Details

We compare results obtained with nonpolarizable[50] and polarizable[51,52] force fields. We use the nonpolarizable extended simple point charge (SPC/E)[50] to keep the connection with our previous works[3,4,10,53-56] and because it continues to be among the leading models in studies of liquid water[57] and field-exposed water in particular. We also consider two polarizable models, the popular and relatively efficient charge-on-spring (SWM4-NDP[51]) model and the more complex BK3 model[52], which combines the Gaussian Charge representation of the earlier GCPM potential[58] with charge mobility of the charge-on-spring models, leading to excellent dielectric properties of this force field[52].

Our simulation cell is a cubic box with lengths of size 24.85 Å, containing 512 water molecules, which corresponds to density of $0.998\ \mathrm{g\ cm^{-3}}$ and results in the ambient pressure in the absence of electric field. Under periodic boundary conditions, the imposition of the static field renders the overall pressure contracting (negative) as already observed elsewhere[5] when using Ewald sums in all three dimensions. We calculate long range electrostatic interactions by a particle-particle particle-mesh solver with a relative error in the per-atom forces of $10^{-5}$ for SPC/E and $10^{-3}$ for BK3 and SWM4-NDP. Tin foil electrostatic boundary conditions are applied in all simulations to offset the internal dielectric screening, thus ensuring the equality between the average field in the sample and the applied electric field.[3,53,59]The application of the field is reflected in anisotropic pressure tensor ($P_{xx}$=$P_{yy}$≠$P_{zz}$, with z axis pointing in the direction of the field), however, we defer quantitative characterization of the pressure behavior to future work. The Lennard-Jones interactions were truncated at the cutoff distance of 12 Å.

The classical equations of motion were solved by the Velocity-Verlet integration with a time step of 1fs. All simulations were performed in the canonical (*NVT*) ensemble at 300 K using Nose-Hoover chain thermostats with a coupling time constant of 30 fs. The relatively short time constant is used for consistency with our parallel studies under alternating (AC) fields. We also performed tests using a CSVR[60] thermostat with equal coupling constant in order to confirm the thermostat choice did not influence the observed dynamics.

The SPC/E and SWM4-NDP simulations were performed using the LAMMPS molecular dynamics simulation package,[61] and the BK3 simulations were carried out with a GROMACS version[62] modified by Marcello-Sega.[63] Equilibration runs lasted 300 ps and all reported averages were collected over a subsequent 500 ps production run, with coordinates written in each timestep.

Spatial distribution function plots were calculated using the TRAVIS software[5364] and plotted using the VMD package[65].

### 2.2. Hydrogen Bond Switching Kinetics

In addition to the original Luzar-Chandler model (section SM-I),[25,26] which focuses on the kinetics phenomenology for describing the dynamics of hydrogen bond breaking and reforming within the first coordination shell, we introduce a modified version that focusses on the kinetics of hydrogen bond *switching*. The rationale behind this change has already been given by Luzar,[26] who noted the breaking of a hydrogen bond is accompanied by the formation of a new bond with a neighboring molecule. The processes of hydrogen bond breaking, diffusion, and formation of a new bond

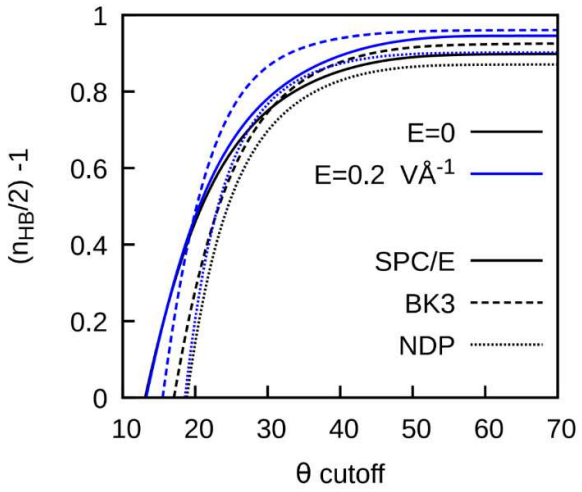


Figure 1. The dependence of the number of H-bonds on the angle cutoff criterion. Although the number of H-bonds is field- and model-dependent, in all cases, $n_{HB}$ plateaus at or before the cutoff angle of $\sim 30^{\circ}$. In this and subsequent figures, we use the abbreviation NDP to denote the SWM4-NDP model.

correspond to a switching of allegiances,[26] a view also emphasized in the extended jump model for water reorientation by Laage and Hynes.[35,66]

In our modified version of the Luzar-Chandler model, we keep the reactive flux formalism,[67,68] but instead of focusing on a *pair* of water molecules, between which hydrogen bonds can form and break (irrespective of which hydrogen is being donated)[25,27], we consider a single, *tagged proton on a* donor water molecule. The distinction becomes increasingly important in the presence of an orienting field because the field directly affects the probability of proton switches between molecules. Instead of calculating the rate of breaking a hydrogen bond between a pair of water molecules, we calculate the rate of switching its H-bonds to a new acceptor. In short, we use the semantics associated with the extended jump model[66] and the methodology presented by Luzar and Chandler model[25,26]

Using $H^*$ and $O^*$ to label the tagged donated hydrogen and the donor oxygen, and $O_a$ and $O_b$ to designate the acceptor molecules before and after a switch, our modified hydrogen bond time correlation function reads

$$c_t(t) = \frac{\langle h_a(t) h_a(0) \rangle}{\langle h_a \rangle} \qquad [1]$$

where $h_a$ equals one if $H^*$ is donated to the initial acceptor $O_a$, and zero otherwise. We use the subscript $t$ to emphasize that unlike the original hydrogen bond time correlation function, $c(t)$ (outlined in the SM), this version applies to a tagged hydrogen atom only. To describe the switching of allegiances, we introduce the second time correlation function:

$$n_s(t) = \frac{\langle h_a(0)\big(1 - H_a(t)\big)h_b\ (t)\rangle}{\langle h_a\rangle}. \qquad [2]$$

Therein, $h_b$ equals one if $H^*$ is donated to a new acceptor $O_b$, and zero otherwise. After a hydrogen has switched its acceptor, the previous acceptor may have left the first shell of the donor molecule or not. Leaving the first solvation shell of the tagged water molecule is necessary for the switch to be complete. The factor $1 - H_a(t)$, where $H_a(t)$ equals one if the previous acceptor is still within the first solvation shell and zero otherwise, has been added to equation [2] to take this diffusion process into account. Thus $n_s(t)$ measures the probability that a complete switching of allegiances has occurred after some time $t$, given that there was an initial hydrogen bond between the donor and the old acceptor at $t = 0$. We use the index $s$, to emphasize the switching process[25] and to distinguish $n_s(t)$ from its original counterpart $n(t)$[25].

Like in the original model,[25] we invoke a phenomenological kinetic scheme to describe the inter-conversion between the different populations associated with $c_t(t)$ and $n_s(t)$:

$$c_t(t) \underset{k_s'}{\overset{k_s}{\leftrightarrows}} n_s(t) \qquad [3]$$

and

$$-\frac{dc_t(t)}{dt} = k_t(t) = k_s c_t(t) - k_s' n_s(t)\ , \qquad \text{for } t > t_{transient} \qquad [4]$$

We can find the best rate constants $k_s$ and $k_s'$ by minimizing deviations between $-\frac{dc_t(t)}{dt}$ and $k_s c_t(t) - k_s' n_s(t)$, which should give a straight line on a correlation plot.

To identify hydrogen bonds, we use geometric criteria[27,69] based on a combination of rules for inter-oxygen separations $d_{O^*\cdots O_a}$, hydrogen-oxygen separations between donor and acceptor molecules $d_{H^*\cdots O_a}$, and hydrogen bond angles $\theta_{H^*-O^*\cdots O_a}$. Using this nomenclature, $d_{O^*\cdots O_a} < 3.5$ Å, which corresponds to the first minimum in the oxygen-oxygen radial distribution function, $d_{H^*\cdots O_a} < 2.4$ Å, which is the corresponding minimum in the oxygen-hydrogen pair correlation function, and $\theta_{H^*-O^*\cdots O_a} < 30°$, which includes about 70% of all hydrogen bonds in all water models, see Figure 1. We use only the distance criterion for $d_{O^*\cdots O_a}$ to identify the first solvation shell of a water molecule, that is, to define $H_a(t)$.

## 3. RESULTS AND DISCUSSION

### 3.1. Structure

In this section, we study the field-induced structure of liquid water (as opposed to work on water clusters, elsewhere)[24]. We are specifically interested in the combined effect of field alignment and local structure preferences of water molecules due to hydrogen bonding. Our results correspond to fixed volume (*NVT*) conditions. While constant pressure calculations with truncated electrostatic interactions indicate the possibility of electro-vaporization for $E$ above 0.4 VÅ$^{-1}$, twice stronger than the fields used here[5,54], a mild electrostriction is observed at fixed chemical potential[3,54], or under fixed presure with Ewald sums *on*[5]. The latter trend is consistent with the contracting pressure observed under the field in the present constant-volume simulations.

We start with the average alignment of water molecules,[3] measured in terms of $\langle \cos \theta_\mu \rangle$, where $\theta_\mu$ is the angle between the dipole moment $\vec{\mu}$ and the static electric field (Figure 2). Initially, the alignment increases almost linearly with the electric field strength. Gradual saturation at fields

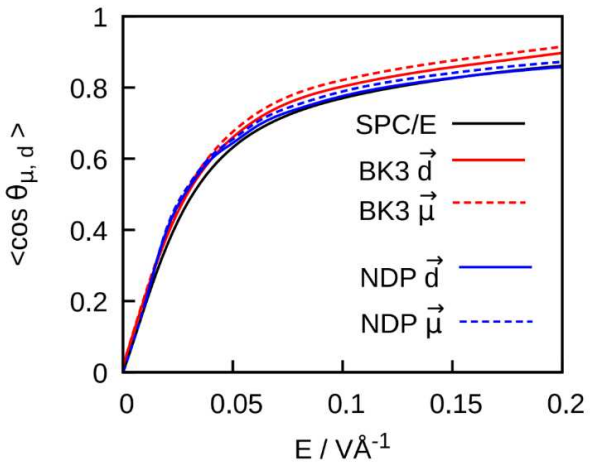


Figure 2. Average alignment of water molecules with the electric field for different water models quantified in terms of the cosine of the angle $\theta$ between the molecular bisector $\vec{d}$ and the electric field, as well as between the dipole moment $\vec{\mu}$ and the electric field.

above 0.01 VÅ$^{-1}$ closely resembles the alignment behavior of free dipoles described by the Langevin-Debye equation[12] indicating only weak resistance from the water structure against such alignment.[3,70-72] For the polarizable models, Figure 2 also includes the average alignment of the molecular bisector $\vec{d}$ measured in terms of $\langle \cos \theta_d \rangle$, where $\theta_d$ is the angle between the bisector and the electric field, showing minute differences from the alignment of the dipoles.

Additional insight can be gained from angle distributions, which we show in Figure 3, both for the angles between the dipole and the electric field $\theta_\mu$ and between an OH bond and the electric field $\theta_{OH}$. Both distributions narrow down with increasing field strength, which simply corresponds to

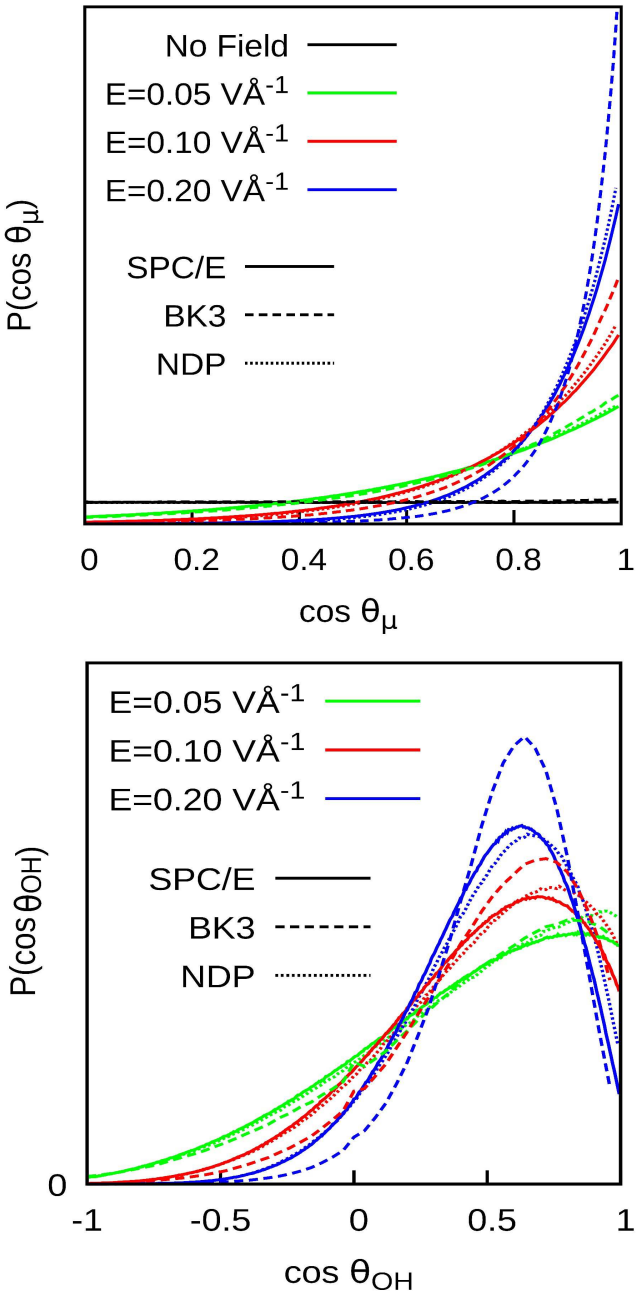


Figure 3. Distributions of orientations of molecular dipoles relative to the field direction, P(cos $\theta_\mu$) (top), and individual OH vectors, P(cos $\theta_{OH}$) under different electric field strengths E for SPC/E, BK3 and SWM4-NDP models of water.

enhanced alignment. In the strong-field limit, however, the two distributions peak at different values. Since the two OH vectors in a molecule form the angle $\alpha_T \sim 109°$, complete field alignment for dipoles ($cos\theta_\mu = 1$) corresponds to only partial alignment of OH bonds with $\theta_{OH} \sim \alpha_T/2$ in all water models. The alignment in BK3 water is comparatively stronger due to a notable increase of its dipole moment under strong electric fields. The alignment of the SWM4-NDP does not differ

significantly from that of SPC/E since, even under the strongest field, the dipole moment $\mu_{SWM4-NDP}^{E=0.2\,V\text{Å}^{-1}} = 2.59\,D$ exceeds $\mu_{\mathrm{SPC/E}}$ $(2.35\,D)$ by only ~10% (Section 3.1.5).

Various metrics have been considered in characterizing intermolecular correlations in liquid water.[73] Previous work has shown that even strong electric fields of $0.2\ \mathrm{V\text{Å}^{-1}}$ cause only insignificant changes in the local tetrahedral structure of the liquid, irrespective of the strong alignment observed above.[54,74] In the following, we confirm this finding by carefully monitoring selected local structural properties of water: radial distribution functions, triplet angle distributions,[75] tetrahedral order parameters,[76] and spatial distribution functions.[77,78]

### 3.1.1. Radial distribution function

Oxygen-oxygen radial distribution functions $g_{\mathrm{OO}}(r)$ reveal only mild field-induced changes in the local structure around SPC/E and SWM4-NDP molecules, while the density amplitudes increase in the case of BK3 water (Figure 4-a). The peak positions, consistent with the unperturbed tetrahedral structure[7,70,79,80] are preserved with all three models. However, structural anisotropies caused by the imposition of the field are smeared in isotropically averaged distribution functions, such as $g_{\mathrm{OO}}(r)$. To alleviate this shortcoming, we consider the distinct cylindrical oxygen-oxygen distribution functions $g_{\mathrm{OO}}(r_{\parallel})$ and $g_{\mathrm{OO}}(r_{\perp})$, where $r_{\parallel}$ and $r_{\perp}$ are the parallel and perpendicular components (with respect to the direction of the electric field) of the oxygen-oxygen distance vector (Figure 4 b, c, and d).

These functions reveal appreciable structural anisotropies, especially in the strongest electric field we consider, $E = 0.2\ \mathrm{V\text{Å}^{-1}}$. With an applied electric field, distributions in field direction exhibit enhanced layering, both in the first and second coordination layer. Correlation functions perpendicular to the electric field, on the other hand, are less structured than their field-free counterparts. Therein, the height of the first coordination shell peak is significantly smaller, whilst the second solvation shell peak is somewhat enhanced. All changes in magnitude are also accompanied by mild shifts in the positions of the corresponding peaks. The general picture that emerges is that upon application of an electric field, first neighbors approach each other in field direction, but are pushed farther in the plane perpendicular to the field.

To explore this concept more carefully, we look at oxygen-oxygen distance distributions between two acceptor water molecules $(\mathrm{A}, \mathrm{A}')$ that receive a hydrogen bond from the same donor molecule, that is, we look at distributions $p_{\mathrm{AA}'}(r_{\parallel})$ and $p_{\mathrm{AA}'}(r_{\perp})$. The distributions and a scheme illustrating this geometry are shown in Figure 5. Without an electric field, these distributions are isotropic. Under the strongest field, however, we see that both acceptors share the same parallel distance to the common donor molecule and that the average distance between both acceptors in the plane

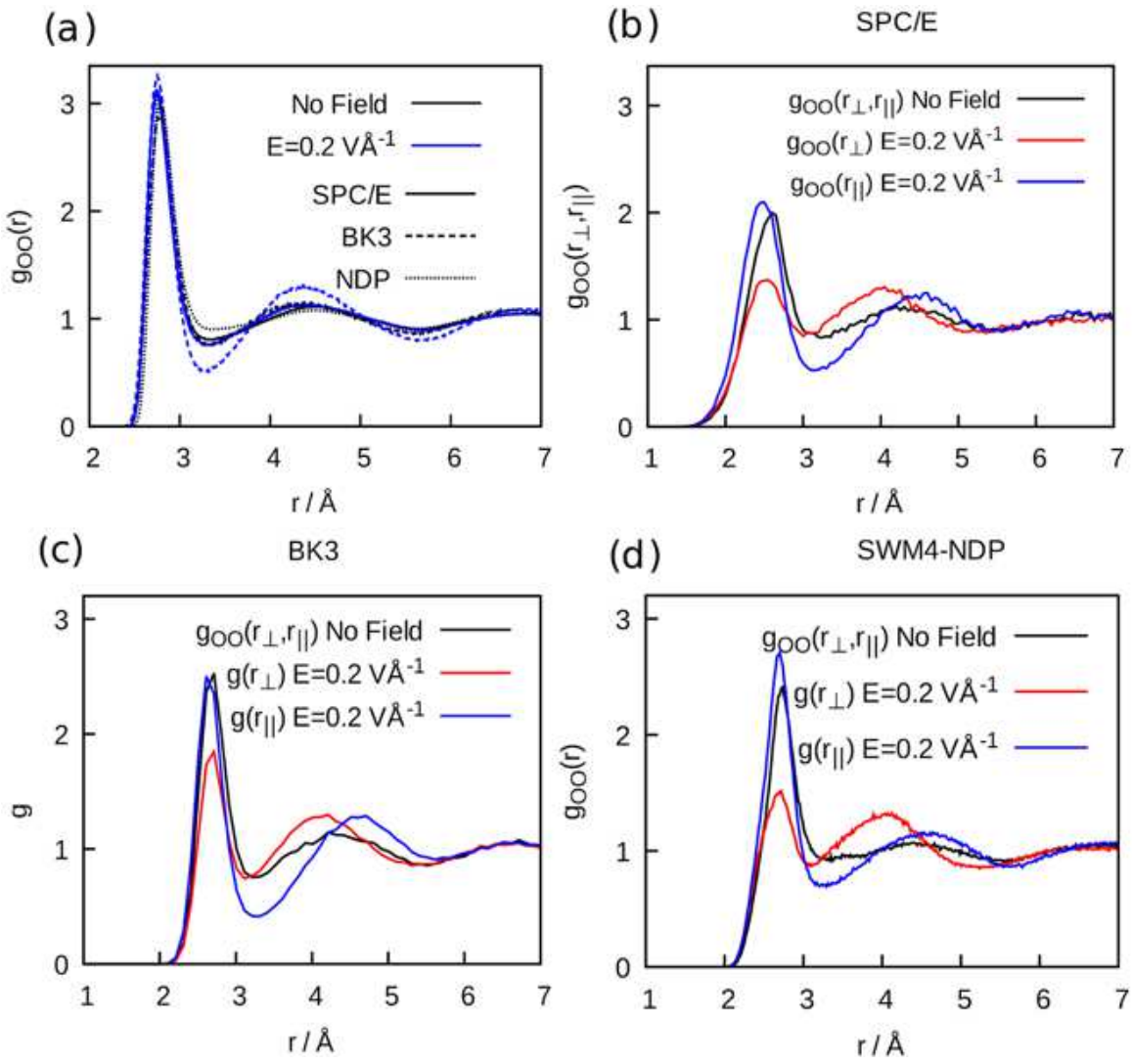


Figure 4. Oxygen-oxygen radial distribution functions $g_{OO}(r)$ for various water models without field and for $E = 0.2$ VÅ$^{-1}$ (a), as well as cylindrical distribution functions in the direction of the E-field $g_{OO}(r_{\parallel})$ and in the plane perpendicular to the E-field $g_{OO}(r_{\perp})$ for SPC/E (b), BK3 (c), and SWM4-NDP water (d) without field and for $E = 0.2$ VÅ$^{-1}$.

perpendicular to the field is about 4 Å, which is the distance of the second peak of $g_{oo}(r_{\perp})$. the common donor molecule and that the average distance between both acceptors in the plane perpendicular to the field is about 4 Å, which is the distance of the second peak of $g_{oo}(r_{\perp})$.

### 3.1.2. Triplet Angle Distributions

An important property for evaluating the tetrahedrality of the water network is the distribution of oxygen triplet angles (Figure 6).[75,81] This distribution is calculated from

$$P(\cos\theta_{OOO}) = \frac{1}{N(n_i - 2)} \left\langle \sum_{i=1}^{N} \sum_{j=1}^{n_i - 1} \sum_{k=j+1}^{n_i} \delta\left(\cos\theta_{OOO} - \frac{r_{ij}.r_{ik}}{|r_{ij}|\,|r_{ik}|}\right) \right\rangle \qquad [5]$$

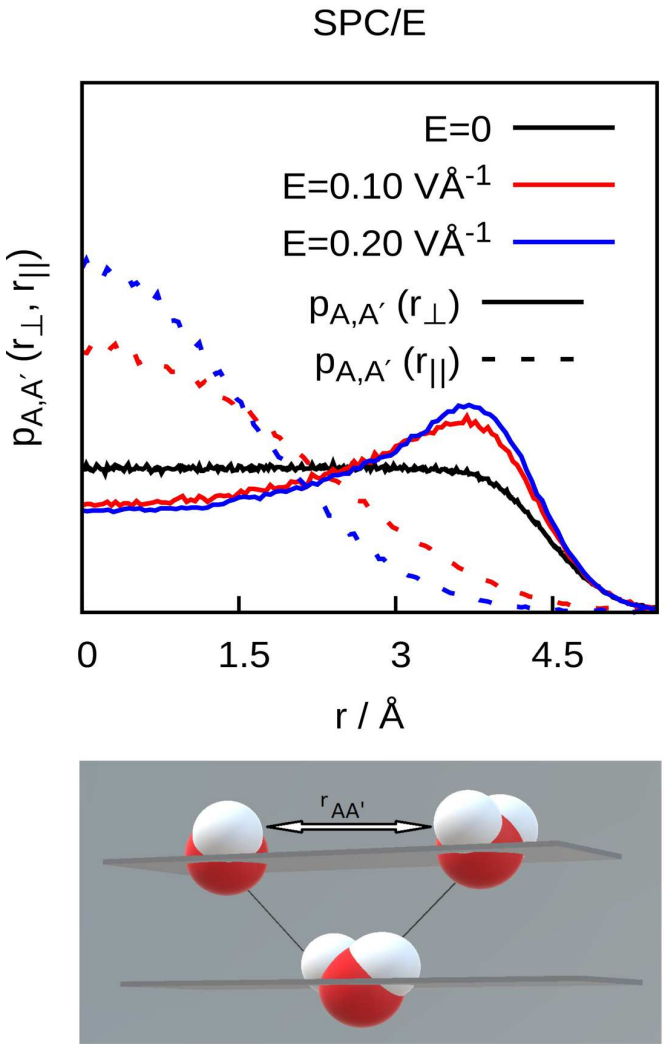


Figure 5. Top panel: Oxygen-oxygen distance distribution functions between two acceptor molecules A and A′ in SPC/E water, $p_{AA'}(r_{\parallel})$ and $p_{AA'}(r_{\perp})$. Results for BK3 and SWM4-NDP water are qualitatively similar (see Figure S 5). Bottom panel: Schematic illustration of the corresponding geometry in strong electric fields. The shift of the dashed plots to the left at increasing E-fields shows that the H-bond acceptors are more likely to be in the same plane.

where $N$ is the total number of molecules, $n_i$ is the number of nearest neighbors (within the first coordination shell) of each molecule i, and $r_{ij}$ and $r_{ik}$ are vectors connecting the central molecule

with two of its closest neighbors. The distributions presented in Fig. 6 feature two peaks corresponding to tetrahedrally coordinated water molecules ($\cos\theta_{OOO} \approx -0.3$) and interstitial ones ($\cos\theta_{OOO} \approx 0.6$).

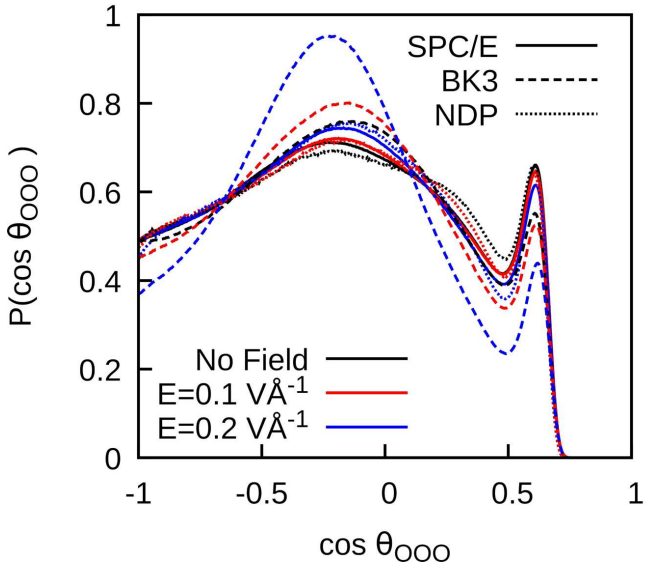


Figure 6. Oxygen triplet angle distributions, see equation [5], in SPC/E, BK3, and SWM4-NDP water under three different E-fields.

In our highest electric fields, the tetrahedral peak of SPC/E, BK3 and SWM4-NDP is raised by about 4%, 25%, and 9% respectively. This change is accompanied by a decrease in the height of the interstitial water peak of about 6%, 20%, and 16%, respectively. The corresponding reduction in the number of interstitial water molecules is consistent with the increased number of hydrogen bonds per water molecule (section 3.1.6). We also observe a minor shift of the tetrahedral peak towards larger angles (smaller $\cos\theta_{OOO}$), that is consistent with the picture developed in Figure 5. Unlike the tetrahedral order parameters (SM Section IV), oxygen triplet distributions take both tetrahedral and translational order into account and are a sensitive probe for the tetrahedrality of the water network Upon increased field strength, they reveal a significant decrease in the number of interstitial water molecules, which are an important part in the hydrogen bond switching mechanism.

### 3.1.3. Average Orientational Correlations

It is also of interest to look at the distance-dependent average orientational correlations measured using the water angle bisector vector $\vec{d}$,

$$g_{dd}(r) = \frac{\langle \vec{d}(0)\vec{d}(r)\rangle}{\langle d\rangle^2}, \qquad [6]$$

which we show in Figure 7. With increasing strength of the field, average orientational correlations increase at all positions, which simply corresponds to increasing average dipolar alignment with the electric field.

An interesting feature of Figure 7 is the second peak of alignment, located at the outer boundary of the 2nd coordination shell (i.e., around 5.2 Å). At such distances, a water molecule experiences only weak angle restrictions due to H-bonding, but is still sufficiently close to the central water molecule to favor the head-to-tail dipole alignment (see Figure 7 right). Under strong E-fields, most of the molecules are aligned with the E-field and the peak vanishes.

### 3.1.4. Spatial Distribution Functions

Spatial distribution functions (SDFs) are a convenient tool to visualize some of the effects discussed above[77,78] by showing the changes in the iso-surfaces of constant local number density of oxygen atoms around the oxygen of a central water molecule typically around 1.3 times the average density in the liquid. Results for SPC/E water are shown in (Figure 8), those for BK3 and SWM4-NDP are given in SM section V. SDFs featuring the first coordination shell show the four lobes typical for liquid water, two corresponding to hydrogen bond donors and two corresponding to hydrogen bond acceptors. The hydrogen bond donor lobes are bridged at the chosen iso-density in Figure 8, and this bridge vanishes upon application of a strong electric field, demonstrating nicely the reduction in the number of interstitial water molecules.

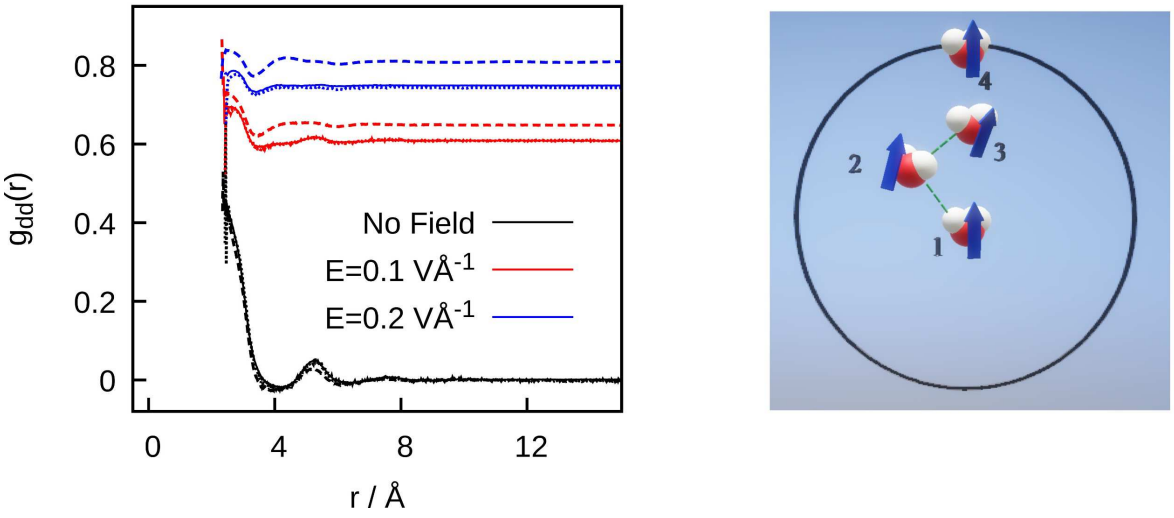


Figure 7. Left: Distance-dependent orientational correlations in SPC/E water (solid lines), BK3 (dashed lines), and SWM4-NDP (dotted lines) under no field and under $E = 0.1$ VÅ$^{-1}$. All models behave qualitatively similarly, although BK3 water molecules are stronger correlated than in other models. Right: A schematic illustration of a possible configuration of H-bonded (2, 3) and non-H-bonded (4) water molecules. Molecule 4 is located at the boundary of the second coordination shell, lacking angular preferences due to H-bonding, which makes it relatively free to rotate.

The second coordination shell is much more affected by the electric field than the first shell. In the second shell, the most probable positions of the neighboring molecules are above the lobes of the first coordination shell. The reason the external E-field is seemingly more influential in the second shell is that the aligning tendency due to the field does not depend on the position while intermolecular forces weaken with increasing separation.

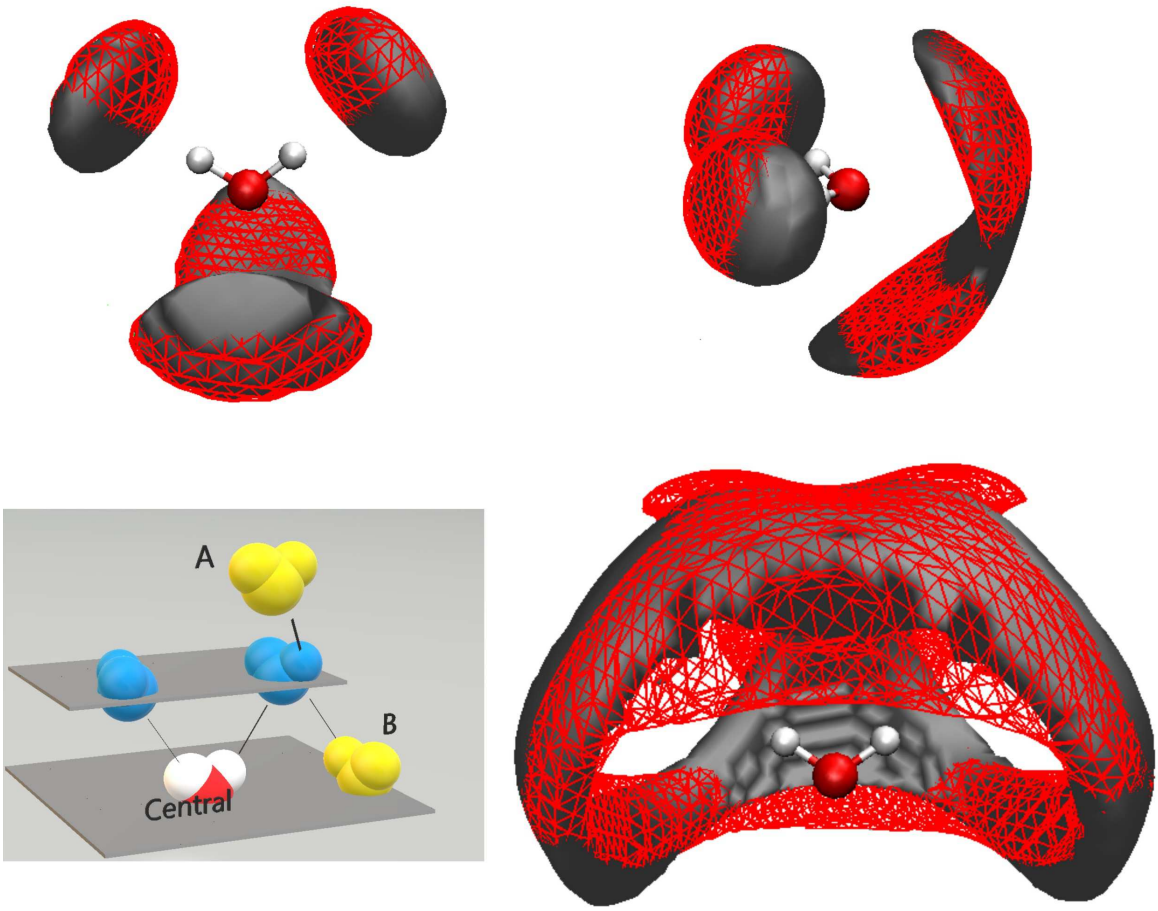


Figure 8. The spatial distribution functions of SPC/E water in the first (top) and the second (bottom right) coordination shell for no field (black) and E = 0.2 VÅ$^{-1}$ (red). The corresponding iso-densities are 1.8 and 1.3, respectively. The central molecules have been added to show the reference coordinate system. (bottom) A schematic of the arrangement of the neighbors under a strong E-field in the first and second coordination shells and the relative position of the molecules that form area A and B in the second shell SDF (bottom left).

As we showed in Figure 4, the water structure is layered in the z-direction, i.e. in the direction of the field under static E-fields, and the neighboring molecules in the second shell in the $x$-$y$ plane are the molecules that share a H-bond donor. These molecules are shown in area B around the

central molecule in Figure 8. Similarly, the second coordination shell molecules located above the central molecule along direction $z$ are spread over a somewhat broader lateral area (area A in Figure 8).

### 3.1.5. Structure of Polarizable Models

The imposition of an electric field does not only align water molecules, but polarizes them as well. Here, we examine the field-induced change in the dipole moments of the polarized water models (Figure 9).

The reported static dipole moment and polarizability volume of BK3 water are $\mu_{BK3} = 2.64$ D and $\alpha_{BK3} = 1.44$ Å$^3$, respectively.[52] Within the linear response regime, the predicted change in the

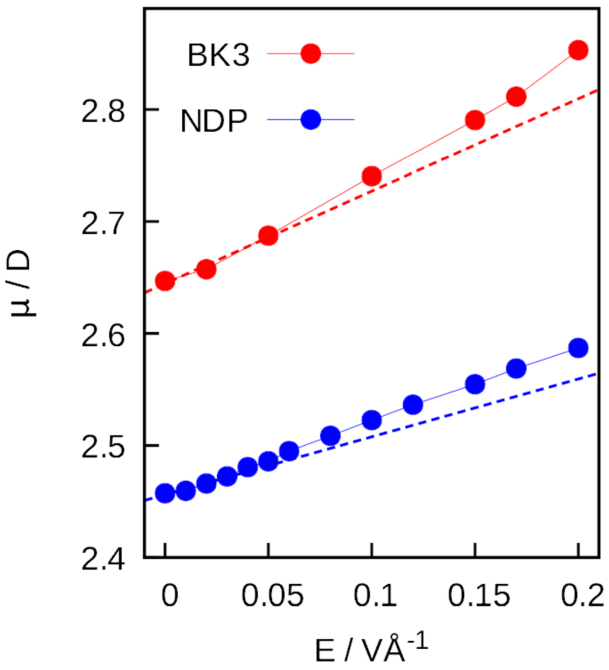


Figure 9. The change in the dipole moment of BK3, and SWM4-NDP water molecules under static electric fields. The dashed lines illustrate a linear trend corresponding to the initial slope $\alpha$ at zero field.

dipole moment upon application of an electric field of strength $0.2\,\text{VÅ}^{-1}$, $\Delta\mu_{BK3}$, should be ~0.1 D, which is ~4% while our results suggest that the dipole moment changes by ~7%. While the low field polarizability resembles that of real water, the use of a

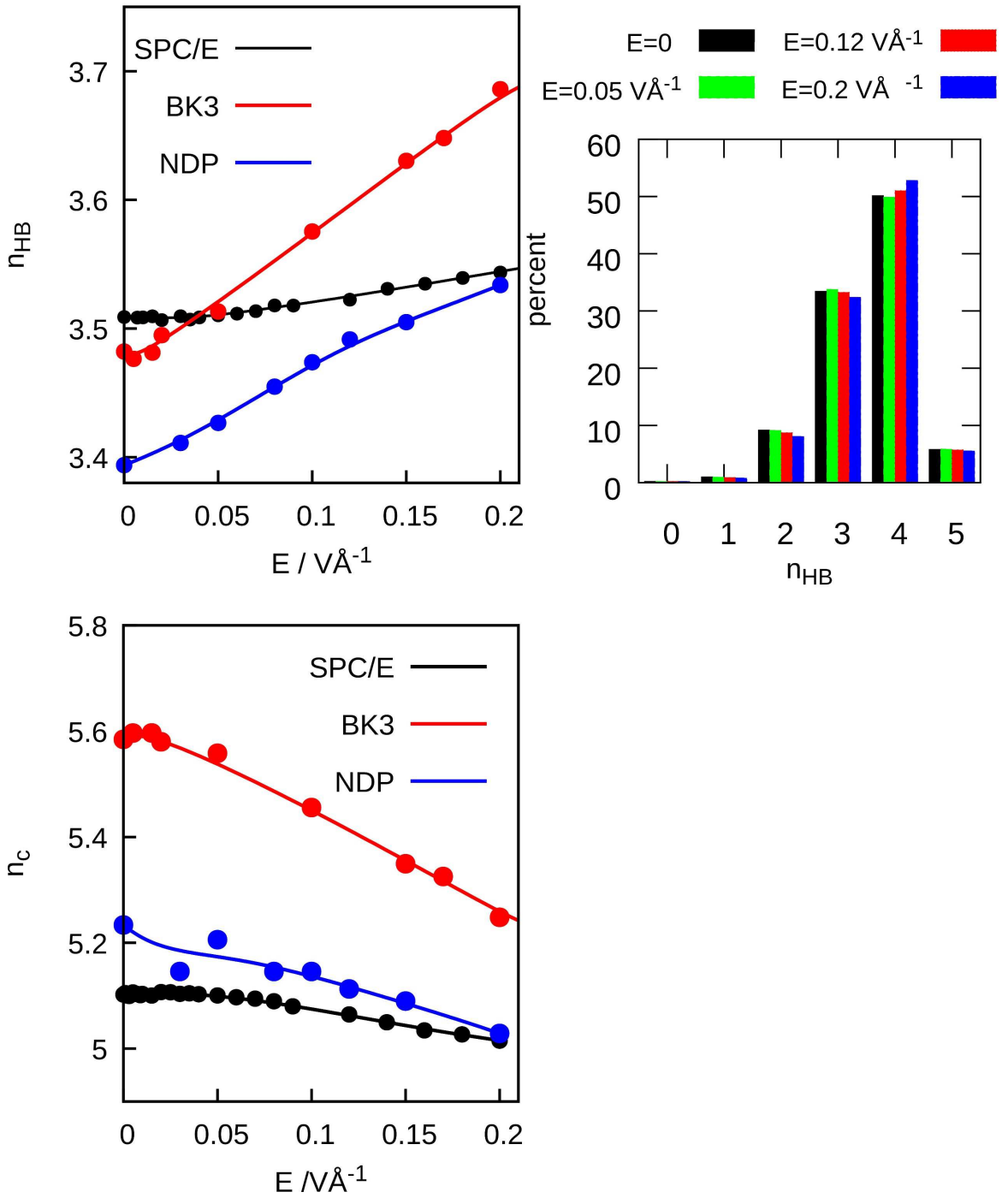


Figure 10. The number of H-bonds (top-left) and the coordination number (bottom) for all water molecules and electric field strengths. The overall change of both values under static fields is small: around 6% for BK3 and less than 1% for SPC/E. Right: The percentage of the water molecules that have a specific number of H-bonds for SPC/E water and selected electric field strengths. In high electric field strengths, there is a very small shift towards tetrahedrally coordinated water. The overall change in the number of H-bonds does not exceed 6%.

suppressed, field dependent polarizability has been suggested to alleviate the nonphysical increase of the dipole moment at stronger E-fields[82], however, the proposed correction becomes significant only at fields well above the strongest field considered in our work.

With the SWM4-NDP model, the nominal polarizability $\alpha_{SWM4-NDP}$ is ~0.98Å$^3$ suggesting a dipole increase $\Delta\mu_{SWM4-NDP} \sim 0.065$ D at $E = 0.2\, V\text{Å}^{-1}$. Results in Fig. 9 show $\mu_{SWM4-NDP}$ to increase from 2.46 D at zero field to ~2.58 D at 0.2 VÅ$^{-1}$, about twice the change expected in a linear response regime. With both polarizable models, the initial slopes in Fig. 9 agree with the nominal polarizabilities (dashed lines in Figure 9) but show positive deviations at stronger fields.

### 3.1.6. Average Number of Hydrogen Bonds

A property with profound implications for the properties of liquid water is the average number of hydrogen bonds $n_{\mathrm{HB}}$ per water molecule, which we study in this section.

In our strongest electric field, the number of hydrogen bonds per water molecule ( Figure 10, top left) increases by about 1%, 6%, and 4% for SPC/E, BK3, SWM4-NDP water, respectively, in good agreement with previous works.[70,71,83,84] The coordination number $n_c$ ( Figure 10, bottom left) decreases by the same fraction and all of these changes are also reflected in the percentage of water molecules that have a specific number of hydrogen bonds ( Figure 10, right).

These results and all quantities discussed so far show consistently that strong dipolar alignment with an electric field does not weaken the tetrahedral water structure. Furthermore, tetrahedrality is not only compatible with field-induced alignment; there is even an increase in in the number of hydrogen bonds per water molecule and a corresponding decrease in the number of interstitial water molecules. These effects are especially pronounced in BK3 and SWM4-NDP water.

## 3.2. Thermodynamics

By looking at various structural properties, we have demonstrated the resilience of the water hydrogen bond network with respect to external electric fields[17,54] In this section, we reinforce this conclusion by studying the thermodynamics of hydrogen bond formation.

We start with a discussion of the average change in the cohesive energy of water $\langle \Delta \mathrm{E}_{\mathrm{coh}} \rangle$, which can be obtained by subtracting the electric field contributions from the change in the total potential energy,

$$\langle \Delta \mathrm{E}_{\mathrm{coh}} \rangle = \langle \Delta \mathrm{E}_{\mathrm{pot}} - \mathrm{E}_{\mathrm{field}} \rangle. \qquad [7]$$

Therein, $E_{\mathrm{field}}$ is easily accessible as $\vec{P} \cdot \vec{E}$, where $\vec{P}$ is the total polarization of the system. The change in cohesive energy ( Figure 11) is almost an order of magnitude smaller than the field-induced potential energy change, with maximum changes of 8.1 kJ/mol in SPC/E, 10.5 kJ/mol in BK3, and 9.1 kJ/mol in SWM4-NDP, under an electric field of 0.2 VÅ$^{-1}$. Once again, we find that the hydrogen bond network is not restrained upon application of an electric field, which would have resulted in a significant increase of the cohesive energy.

Additionally, average numbers of hydrogen bonds allow us to estimate the standard free energy of hydrogen bond formation $\Delta G^{\circ}_{\mathrm{HB}}$ from the fraction of intact bonds $r$:

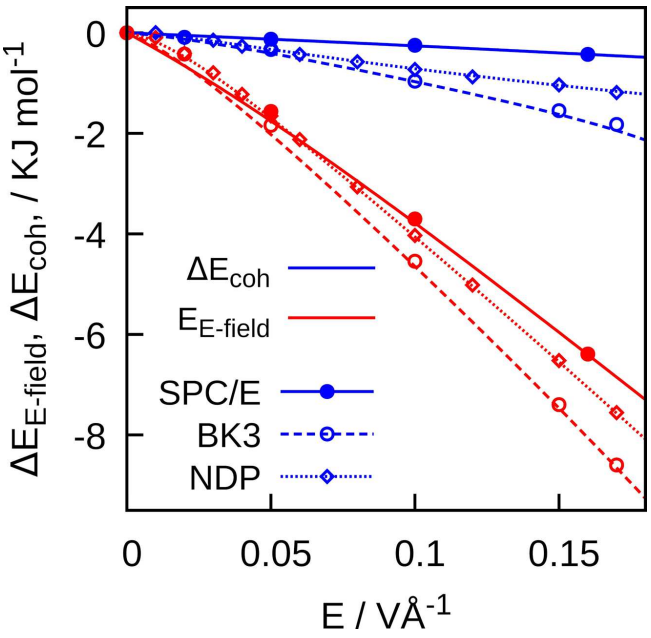


Figure 11. Changes in average cohesive and electric field energy of the system, $\langle \Delta E_{coh} \rangle$ and $\langle E_{field} \rangle$, with and electric field for various water models. For $E = 0$, $E_{coh}^{SPC/E} = -46.6$ kJ mol$^{-1}$, $E_{coh}^{BK3} = -43.4$ kJ mol$^{-1}$, and $E_{coh}^{SWM4-NDP} = -43.3$ kJ mol$^{-1}$.

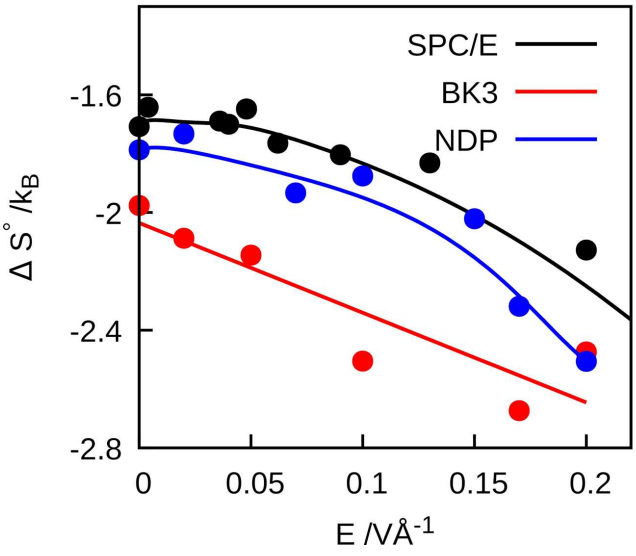


Figure 12. Reduction of the standard entropy of a H-bond calculated from the slope of standard free energy versus temperature plot in SPC/E, SWM4-NDP, and BK3 water with increasing electric field strength. The temperature ranges from 260 K to 330 K.

$$r = \frac{e^{-\beta \Delta G^{\circ}_{\mathrm{HB}}}}{e^{-\beta \Delta G^{\circ}_{\mathrm{HB}}} + 1}. \qquad [8]$$

where $\beta = 1/k_B T$. A water molecule having 5 or more hydrogen bonds is an unlikely scenario that happens only briefly during hydrogen bond switching, see the histogram in Figure 9.[66] Assuming the maximum number of stable H-bonds per molecule to be four[1] $\left(r = \frac{n_{HB}}{4}\right)$, we calculated standard free energies of hydrogen bond formation for all three water models listed in Table 1.

Table 1. The standard free energy of hydrogen bond formation from eq. [8].

| Water model | E-field | $\beta \Delta G^{\circ}$ |
|---|---|---|
| SPC/E | 0 | -1.94 |
| | 0.2 $V$Å$^{-1}$ | -2.04 |
| BK3 | 0 | -1.90 |
| | 0.2 $V$Å$^{-1}$ | -2.46 |
| SWM4-NDP | 0 | -1.72 |
| | 0.2 $V$Å$^{-1}$ | -2.02 |

We have also run our simulations in a range of temperatures between 275 K and 320 K, and have computed the standard entropies of bond formation $\Delta S^{\circ}_{\mathrm{HB}}$ from the slope $-d\Delta G^{\circ}_{\mathrm{HB}}/\mathrm{d}T$.

The entropic penalty for the formation of hydrogen bonds increases with the electric field strength. In SPC/E water, ~20% reduction of $\Delta S^{\circ}_{\mathrm{HB}}$ due to the field $E =$ 0.2 VÅ$^{-1}$ accompanies a small, ~1% *increase* in the number of hydrogen bonds as bonding *energy* strengthens with the field.

## 3.3. Dynamics

### 3.3.1. Hydrogen bond kinetics

We studied hydrogen bond kinetics using both the original Luzar-Chandler model (see SM) and the modified version introduced in section 2.2. Recall that the former describes this kinetics through rate constants $k$ and $k'$ associated with hydrogen bond *breaking and reforming*, whereas the latter employs the rate constants $k_s$ and $k'_s$ associated with hydrogen bond *switching* (forth and back).

The original functions $c(t)$ and $n(t)$ are shown in Figure S 1, and the *tagged-hydrogen* $c_t(t)$ and $n_s(t)$ are plotted in Figure 13. Regardless of the field, the relaxation of hydrogen bond populations in polarizable water models is slower than in non-polarizable ones. Furthermore, electric field effects are generally stronger in polarizable models than in the nonpolarizable ones.

The validity of both models can be assessed by examining the correlation plots of $k(t) = -dc/dt$ vs. $kc(t) - k'n(t)$ and $k_t(t) = -dc_t/dt$ vs. $k_s c_t(t) - k'_s n_s(t)$, respectively. These correlation

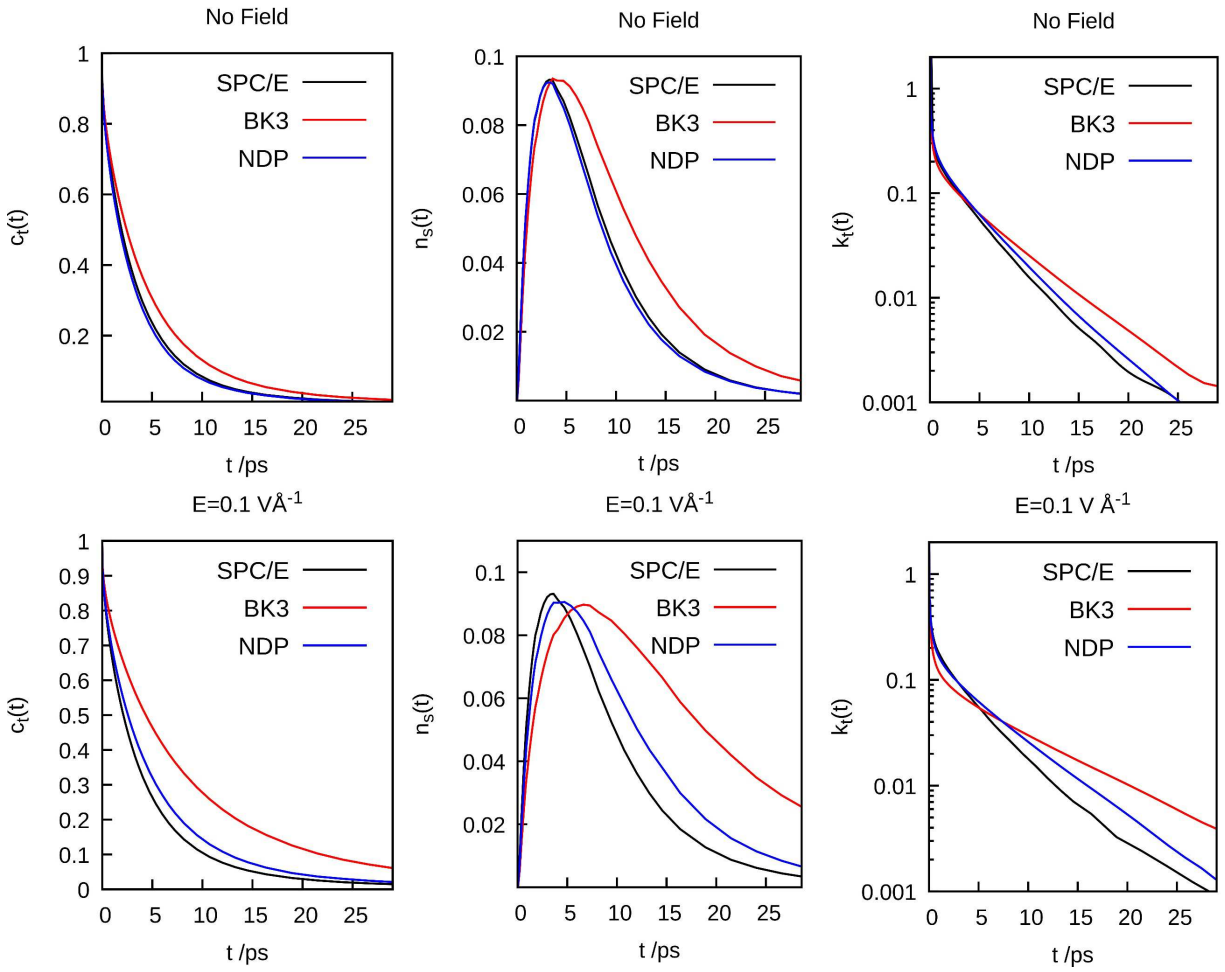


Figure 13. The hydrogen bond correlation functions. (left) tagged hydrogen correlation function, $c_t(t)$ (eq. [1]), (middle) hydrogen bond switching correlation function, $n_s(t)$ (eq. [2]), and (right) the relaxation of a tagged hydrogen bond $k_t(t) = -dc_t/dt$ for various water models under zero field (top) and E = 0.1 VÅ$^{-1}$ (bottom).

plots are presented in Figure 14 and show that both models are suitable for describing the hydrogen bond kinetics on timescales where they can be expected to hold (i.e., beyond the initial transient regime) for selected field strengths (as well as further dynamical quantities, to be discussed shortly).

By looking closer at the field-dependence of all rate constants Figure 15, we notice that the forward rate constant of switching $k_s$ is always lower than the breaking rate constant $k$. In other words, breaking of hydrogen bonds is more frequent than complete switching of allegiances, since unlike switching, breaking may also result in transient states corresponding to interstitial water molecules. In return, the rate constant of reforming $k'$ is always larger than the backward rate constant of switching $k_s'$ These results are consistent with the observation of dangling bonds from 2D IR spectroscopy.[85,86] In BK3, differences between the original, tagged-pair and modified, tagged-proton

rate constants diminish with increasing field strength, which is consistent with the decrease in the number of interstitial water molecules discussed in section 3.1.2.

Furthermore, we can identify two distinct dynamical regimes. In fields with a strength of less than $0.025$ VÅ$^{-1}$, both $k$ and $k_s$ increase with rising electric field strengths. Beyond such fields, they decrease. These effects are model-independent, although most pronounced in BK3 and least apparent in SWM4-NDP. Thus, the field alignment does have an accelerating influence on hydrogen bond breaking and switching kinetics, if the fields are small enough to not meet significant resistance from the water network (compare average alignment, Figure 2) and a decelerating influence in stronger fields.

A careful analysis of the rate constants of reforming reveals further differences between the various models. For SPC/E, these rate constants increase in the high-field regime, whereas for SWM4-NDP and BK3, they decrease. In other words, in SPC/E, transiently broken hydrogen bonds are

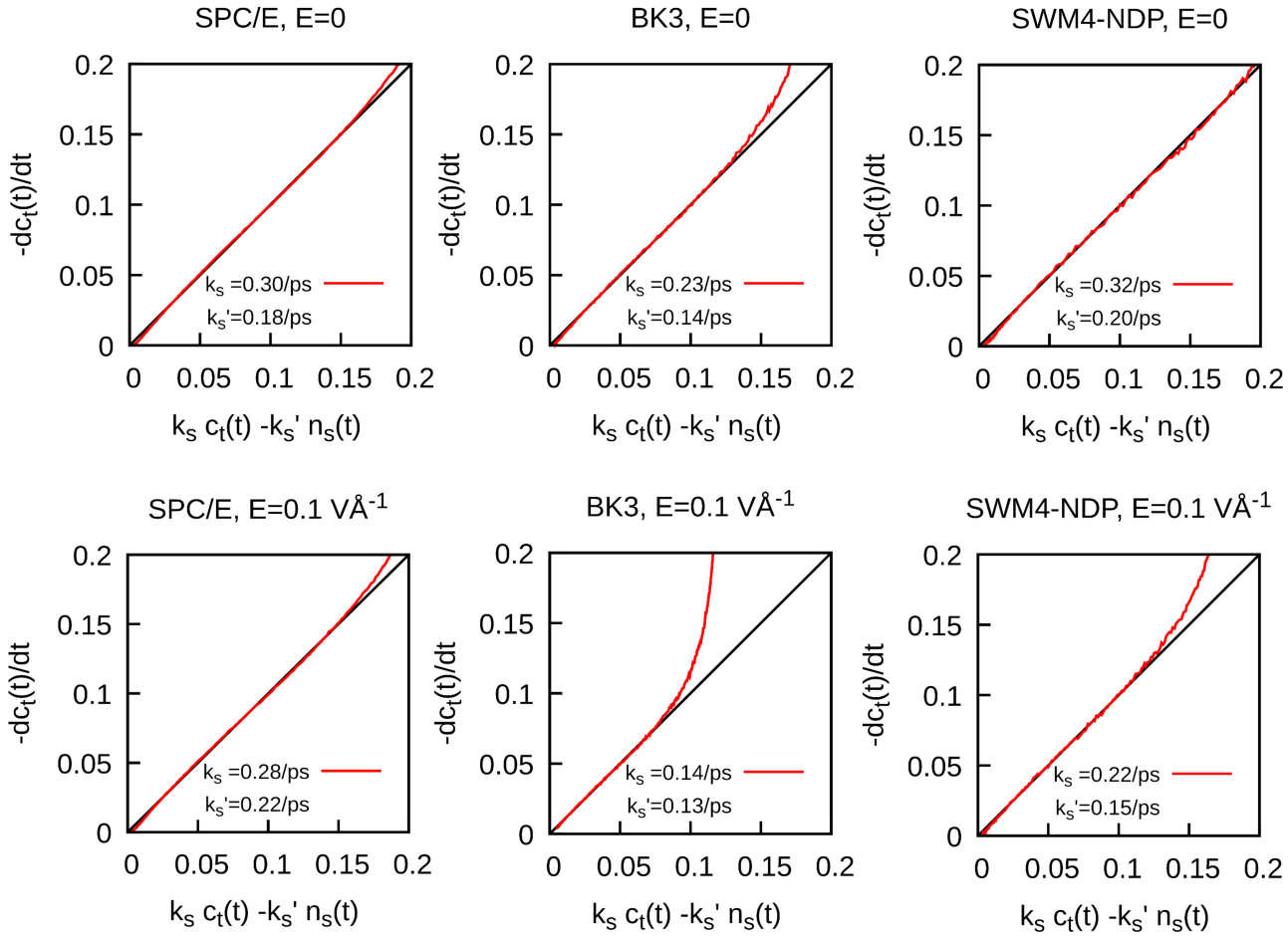


Figure 14. Hydrogen bond switching correlation plots showing the best fit between $k_t(t)$ and $k_s\, c(t) - k_s' n_s(t)$ to find the a pair of rate constants $k_s$ and $k_s'$ in SPC/E (left), BK3 (middle) and SWM4-NDP (right) for zero field (top) and $E = 0.1$ VÅ$^{-1}$(bottom).

more likely to reform with increasing field strength, whereas in the polarizable models, they are less likely. In combination with the decreasing rate constants of hydrogen bond breaking, this indicates that hydrogen bonds in SWM4-NDP and BK3 are stronger. This finding is reinforced by the average number of hydrogen bonds and their free energies of formation, respectively (sections

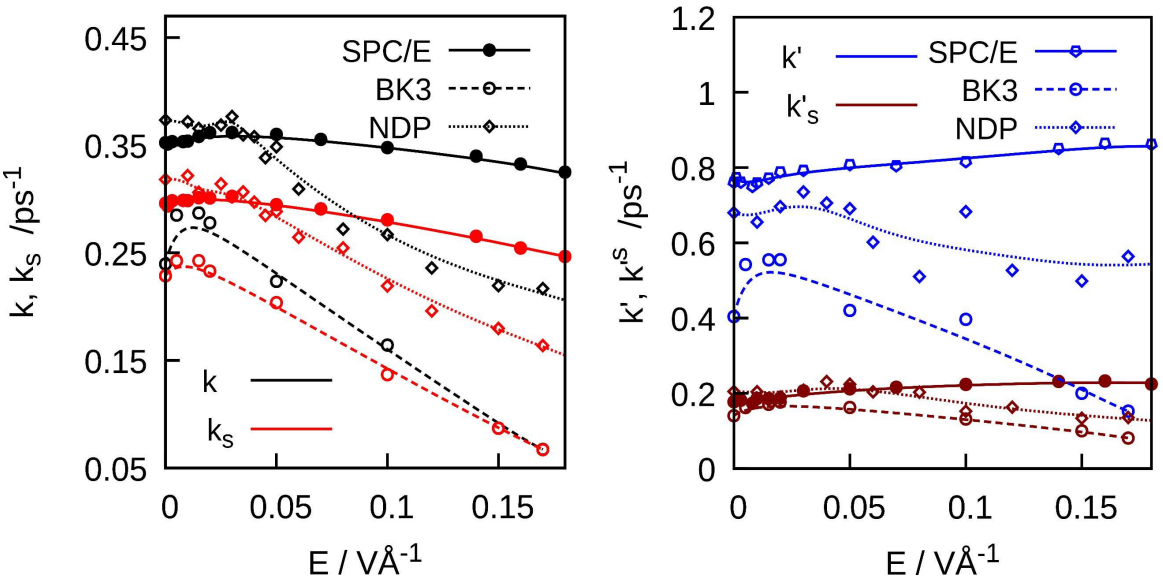


Figure 15. The rate constants of hydrogen bond breaking k and switching $k_s$ (top, left), as well as the rates of H-bond reforming, $k'$ and switching back $k'_s$ (top, right) for three water models under electric fields ranging from 0 to 0.18 VÅ$^{-1}$. Lines are meant to guide the eye.

3.1.6 and 3.2). The same discussion applies to the rate constants of the revised model.

Confirmation for increased hydrogen bond strength in BK3 can also be seen in the transient regime of $k(t)$, which we show in Figure 16. This regime features the contributions of the librations-induced decay of the hydrogen bond populations, which is larger in BK3 than with either of the two other models. A deeper first dip corresponds to a stronger restoring force.

### 3.3.2. Diffusion

We now proceed by using the modified model to correlate H-bond kinetics with diffusion.

Using the Einstein relation, we calculated self-diffusion coefficients of water from the slope of the mean squared displacement over time between 50 and 70 ps, see Figure 17. Self-diffusion is reduced from ~20% in SPC/E water to close to 80% in BK3, respectively, under our strongest electric field of 0.2 VÅ$^{-1}$.

We study in-field and perpendicular diffusion coefficients $D_{\parallel}$ and $D_{\perp}$, separately, and observe an appreciable anisotropy. In SPC/E water, diffusion perpendicular to the electric field accelerates up to 0.03 VÅ$^{-1}$, reaches a maximum, and slows-down again in higher fields. In BK3 water, the perpendicular components of the diffusion tensor decrease monotonously. We see a maximum in the

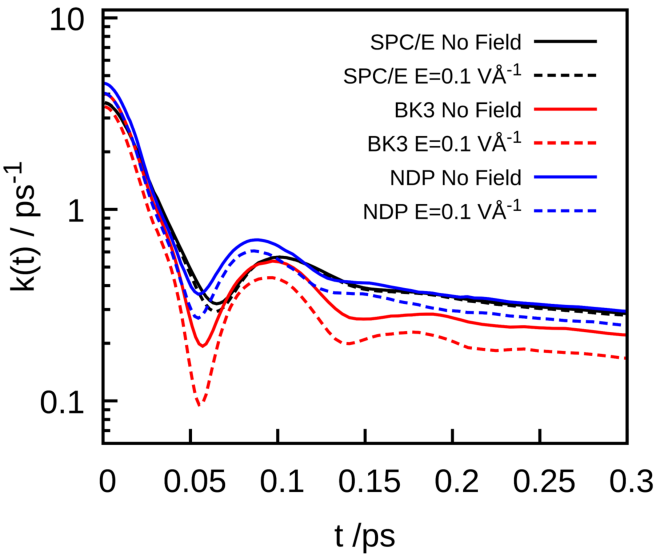


Figure 16. The time dependence of the rate of relaxation to equilibrium, $k(t) = -dc(t)/dt$ within the transient regime for SPC/E, BK3 and SWM4-NDP water models under zero field and E = 0.1 VÅ$^{-1}$.

overall diffusion of SPC/E water at $E \sim 0.03$ VÅ$^{-1}$, and in BK3 and SWM4-NDP models around 0.01 VÅ$^{-1}$. Increasing the alignment of water molecules, increases the rate of H-bond breaking, see Figure 15, but since the diffusion of molecules parallel to the E-field is limited, the diffusion increases only perpendicular to the E-field. Thus, our results are in contrast to those of Jung et al.,[74] who report that the self-diffusion diffusion is higher along the field direction than perpendicular to it. However, they studied water at quite different conditions, notably $T = -30$ °C and $E = 0.5\ V$Å$^{-1}$.

Diffusion coefficients can be related to the observed hydrogen bond kinetics. The self-diffusion process in water can be approximated by a random walk, characterized by the relation[87]

$$D = \frac{a_s^2}{6\tau_{\text{step}}}, \qquad [9]$$

where $\tau_{\text{step}}$ is the characteristic time between diffusive steps and $a_s$ is the corresponding step length. Diffusive steps happen only after a complete switching of allegiances. Thus, the frequencies of diffusion steps and switching must be equal:

$$\frac{1}{\tau_{\text{step}}} = \mathrm{k}_s. \qquad [10]$$

Using the equations [9] and [10], we have fitted diffusion coefficients to switching rates by adjusting the diffusive step length $a_s$. We obtain an excellent agreement between these different kinds of data using an essentially identical value of $a_s \sim 2.3$ Å for all the three models (optimal fits are obtained using $a_s = 2.27$ Å in SPC/E water, 2.33 Å in BK3 water, and 2.28 Å in SWM4-NDP water). These results demonstrate nicely the tight connection between diffusion and hydrogen bond dynamics,[88] as well as the applicability of our modified kinetic scheme for studying this connection over a wide range of electric fields. Such correlation does not exist between the diffusion coefficient and the rate of H-bond breaking, $k$ since breaking a H-bond does not always result in a diffusive step, and the molecule needs to find a new acceptor to switch and then jump the H-bond area of the new acceptor.[66]

Figure 17 shows that the change in the overall diffusion is correlated with the change in $k_s$ rather than $k$, whereas $D_\perp$ is well correlated with $k$ in SPC/E water, and partially so in the cases of the polarizable models. We explain these correlations by noting that in a plane perpendicular to the E-field, the breaking of a H-bond can easily result in switching of the bond to a newer acceptor, and diffusion of the water molecule. This is not the case with diffusion in the direction z, parallel to E-field, as the field hinders rotations reducing the dipole alignment, and the molecules cannot move between the layers, while they can comparatively easily break their bonds through rotations around the axis parallel to the field and translate along the x-y plane. So, parallel to the field, breaking of H-bonds is associated with a smaller probability of switching the H-bond. The E-field affects $D_\parallel$ and $k_s$ equally, so the overall diffusion remains correlated with $k_s$ but not with $k$.

## 4. CONCLUDING REMARKS

We applied a range of static electric fields to bulk water. First, we examined the change in the structure of water by looking at different structure functions. Radial distribution functions, oxygen triplet angle distributions, and tetrahedral order parameters show that the tetrahedral structure of water survives and even strengthens under an electric field. Angle-averaged radial distributions show only minor field-induced changes in the first coordination shell. The effect of the field is more visible in the second shell, where the correlations with the central molecule are comparatively weaker and easier to perturb. However, distribution functions along distinct directions, parallel with or perpendicular to the field, reveal significant structural anisotropies. Specifically, local structure appears enhanced along the direction of the field, a feature consistent with impeded diffusive dynamics parallel to the field.

Furthermore, we have extended our hydrogen bond kinetics model[25] to consider tagged proton bonds and to calculate the rate of hydrogen bond switching.[26,35] Polarizable[85] water models show considerably slower hydrogen bond dynamics than non-polarizable ones. Electric fields slow down the hydrogen bond switching process[89] and we give a detailed explanation: (1) Limited orientational freedom favors reforming transiently broken hydrogen bonds rather than switching

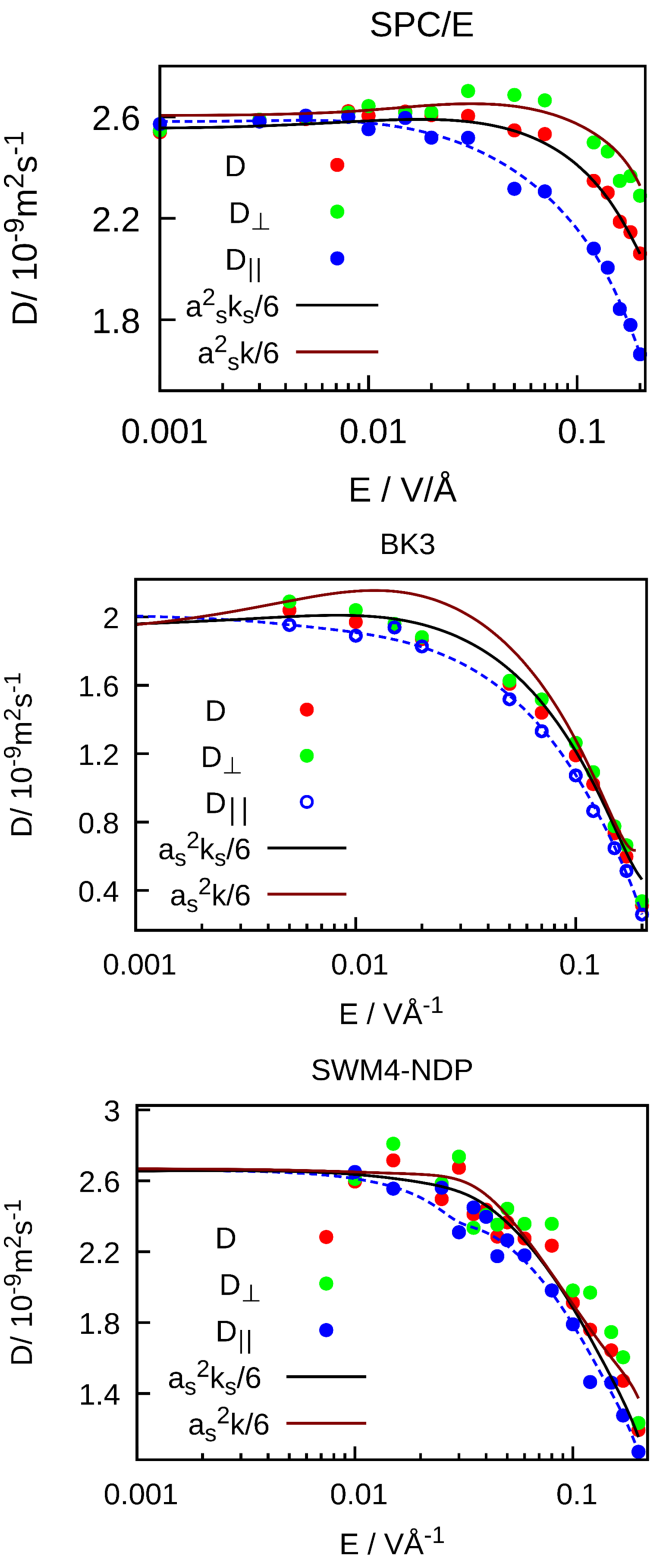


Figure 17. Isotropic diffusion coefficients $D$ as well as the parallel $D_{\|}$ and perpendicular components $D_{\perp}$ of the diffusion tensor in SPC/E water (top), BK3 water (middle), and SWM4-NDP water(bottom). The black and brown lines represent the best fits of the overall and perpendicular diffusion coefficients to a random walk characterized by the frequency of H-bond switching and breaking, respectively. The blue line serves as guide to the eye. A log-scale is used on the x-axes to emphasize the weak field behavior. For non-logarithmic plots see Figure S 3.

to a new acceptor. (2) The strength of hydrogen bonds increases with the electric field. (3) Acceptor switching and the translation of water molecules are highly correlated and decelerated hydrogen bond switching also reduces the translational mobility of water molecules.[2,90] The effect of the field on translational diffusion shows a considerable anisotropy with greater reduction observed in the diffusivity along the direction of the field. Interestingly, the notable dynamic anisotropy observed in the nonpolarizable force field is much less pronounced with polarizable water models.

The formalism we used was designed for studies of water under a static electric field but is equally applicable to time varying fields and we will report on the analysis of structure and dynamics of water under AC fields in a subsequent article.

## SUPPLEMENTARY MATERIAL

See supplementary material for an outline of the original hydrogen bond kinetics formalism[25] and the corresponding results for hydrogen bond time correlation functions, hydrogen bond kinetics correlation plots, the relation between these kinetics and anisotropic diffusivities, tetrahedral order parameters, $g_{OH}$ and $g_{HH}$ radial distribution functions, and spatial and directional distribution functions under the influence of electric field.

## ACKNOWLEDGMENT

This work was supported by the U.S. Department of Energy, Office of Basic Sciences (DE-SC 0004406) in the early stage, and by the National Science Foundation (CHE-1800120) in the late stage. We also acknowledge supercomputing time allocations from the Extreme Science and Engineering Discovery Environment (XSEDE), supported by NSF Grant No. OCI-1053575, and the National Energy Research Scientific Computing Center (NERSC), supported by the Office of Science of the U.S. Department of Energy (DEAC02-05CH11231).

## REFERENCES

[1]D. Eisenburg and W. Kauzmann, *The structure and properties of water*. (Oxford Univ. Press, London, 2005).
[2]Z. Futera and N. J. English, Communication: Influence of external static and alternating electric fields on water from long-time non-equilibrium ab initio molecular dynamics, *J. Chem. Phys.* **147**, 031102 (2017).
[3]D. Vanzo, D. Bratko, and A. Luzar, Nanoconfined water under electric field at constant chemical potential undergoes electrostriction, *J. Chem. Phys.* **140**, 074710 (2014).
[4]D. Bratko, C. D. Daub, K. Leung, and A. Luzar, Effect of field direction on electrowetting in a nanopore, *J. Am. Chem. Soc.* **129**, 2504 (2007).
[5]J. L. England, S. Park, and V. S. Pande, Theory for an order-driven disruption of the liquid state in water, *J. Chem. Phys.* **128**, 044503 (2008).
[6]P. Kumar and S. H. Han, Dynamics of two-dimensional monolayer water confined in hydrophobic and charged environments, *J. Chem. Phys.* **137**, 114510 (2012).
[7]D. Y. Zong, H. Hu, Y. Y. Duan, and Y. Sun, Viscosity of water under electric field: Anisotropy induced by redistribution of hydrogen bonds, *J. Phys. Chem. B* **120**, 4818 (2016).

[8]S. De Luca, B. D. Todd, J. S. Hansen, and P. J. Daivis, Molecular dynamics study of nanoconfined water flow driven by rotating electric fields under realistic experimental conditions, *Langmuir* **30**, 3095 (2014).
[9]N. J. English, Molecular dynamics simulations of microwave effects on water using different long-range electrostatics methodologies, *Mol. Phys.* **104**, 243 (2006).
[10]C. D. Daub, D. Bratko, and A. Luzar, Nanoscale wetting under electric field from molecular simulations, *Topics Curr. Chem.* **307**, 155 (2012).
[11]N. J. English and C. J. Waldron, Perspectives on external electric fields in molecular simulation: Progress, prospects and challenges, *Phys. Chem. Chem. Phys.* **17**, 12407 (2015).
[12]G. Sutmann, Structure formation and dynamics of water in strong external electric fields, *J. Electroanal. Chem.* **450**, 289 (1998).
[13]M. A. Saitta, F. Saija, and P. Giaquinta, Ab initio molecular dynamics study of dissociation of water under an electric field, , *Phys. Rev. Lett.* **108**, 207801 (2012).
[14]A. Vegiri, Translational dynamics of a cold water cluster in the presence of an external uniform electric field, *J. Chem. Phys.* **116**, 8786 (2002).
[15]A. Vegiri, Reorientational relaxation and rotational-translational coupling in water clusters in a d.C. External electric field, *J. Mol. Liq.* **110**, 155 (2004).
[16]A. Amadei, M. E. F. Apol, G. Brancato, and A. Di Nola, Theoretical equations of state for temperature and electromagnetic field dependence of fluid systems, based on the quasi-gaussian entropy theory, *J. Chem. Phys.* **116**, 4437 (2002).
[17]J. L. Aragones, L. G. MacDowell, J. I. Siepmann, and C. Vega, Phase diagram of water under an applied electric field, *Phys. Rev. Lett.* **107**, 155702 (2011).
[18]N. J. English and J. M. D. MacElroy, Hydrogen bonding and molecular mobility in liquid water in external electromagnetic fields, *J. Chem. Phys.* **119**, 11806 (2003).
[19]N. J. English and J. M. D. MacElroy, Molecular dynamics simulations of microwave heating of water, *J. Chem. Phys.* **118**, 1589 (2003).
[20]A. Vegiri, Dynamic response of liquid water to an external static electric field at t=250 k, *J. Mol. Liq.* **112**, 107 (2004).
[21]M. Tanaka and M. Sato, Microwave heating of water, ice, and saline solution: Molecular dynamics study, *J. Chem. Phys.* **126**, 034509 (2007).
[22]S. Acosta-Gutierrez, J. Hernandez-Rojas, J. Breton, J. M. G. Llorente, and D. J. Wales, Physical properties of small water clusters in low and moderate electric fields, *J. Chem. Phys.* **135** (2011).
[23]J. Hernandez-Rojas, B. S. Gonzalez, T. James, and D. J. Wales, Thermodynamics of water octamer in a uniform electric field, *J. Chem. Phys.* **125**, 1 (2006).
[24]Y. C. Choi, C. Pak, and K. S. Kim, Electric field effects on water clusters (n=3-5): Systematic ab initio study of structures, energetics, and transition states, *J. Chem. Phys.* **124**, 094308 (2006).
[25]A. Luzar and D. Chandler, Hydrogen-bond kinetics in liquid water, *Nature* **379**, 55 (1996).
[26]A. Luzar, Water hydrogen-bond dynamics close to hydrophobic and hydrophilic groups, *Faraday Discuss.* **103**, 29 (1996).
[27]A. Luzar, Resolving the hydrogen bond dynamics conundrum, *J. Chem. Phys.* **113**, 10663 (2000).
[28]J. D. Eaves, J. J. Loparo, C. J. Fecko, S. T. Roberts, A. Tokmakoff, and P. L. Geissler, Hydrogen bonds in liquid water are broken only fleetingly, *Proc. Natl. Acad. Sci.* **102**, 13019 (2005).
[29]J. Teixeira, A. Luzar, and S. Longeville, Dynamics of hydrogen bonds: How to probe their role in the unusual properties of liquid water, *J. Phys.: Condens. Matter* **18**, S2353 (2006).
[30]J. Chowdhary and B. M. Ladanyi, Surface fluctuations at the liquid-liquid interface, *Phys. Rev. E* **77**, 4045 (2008).

[31]I. Benjamin, Hydrogen bond dynamics at water/organic liquid interfaces, *J. Phys. Chem. B* **109**, 13711 (2005).
[32]N. Winter, J. Vieceli, and I. Benjamin, Hydrogen-bond structure and dynamics at the interface between water and carboxylic acid-functionalized self-assembled monolayers, *J. Phys. Chem. B* **112**, 227 (2008).
[33]S. Paul and A. Chandra, Hydrogen bond dynamics at vapour-water and metal-water interfaces, *Chem. Phys. Lett.* **386**, 218 (2004).
[34]A. A. Milischuk and B. M. Ladanyi, Structure and dynamics of water confined in silica nanopores, *J. Chem. Phys.* **135**, 174709 (2011).
[35]D. Laage and J. T. Hynes, A molecular jump mechanism of water reorientation, *Science* **311**, 832 (2006).
[36]D. Laage, G. Stirnemann, and J. T. Hynes, Water reorientation in the hydration shells of hydrophilic and hydrophobic solutes, *Science China-Physics Mechanics & Astronomy* **53**, 1068 (2010).
[37]F. Paesani, S. Yoo, H. J. Bakker, and S. S. Xantheas, Nuclear quantum effects in the reorientation of water, *J. Phys. Chem. Lett.* **1**, 2316 (2010).
[38]D. Laage and W. H. Thompson, Reorientation dynamics of nanoconfined water: Power-law decay, hydrogen-bond jumps, and test of a two-state model, *J. Chem. Phys.* **136** (2012).
[39]P. Liu, E. Harder, and B. J. Berne, Hydrogen-bond dynamics in the air-water interface, *J. Phys. Chem. B* **109**, 2949 (2005).
[40]V. K. Yadav and A. Chandra, First-principles simulation study of vibrational spectral diffusion and hydrogen bond fluctuations in aqueous solution of n-methylacetamide, *J. Phys. Chem. B* **119**, 9858 (2015).
[41]G. Stirnemann, P. J. Rossky, J. T. Hynes, and D. Laage, Water reorientation, hydrogen-bond dynamics and 2d-ir spectroscopy next to an extended hydrophobic surface, *Faraday Discuss.* **146**, 263 (2010).
[42]J. Chowdhary and B. M. Ladanyi, Molecular simulation study of water mobility in aerosol-ot reverse micelles, *J. Phys. Chem. A* **115**, 6306 (2011).
[43]E. M. Stuve, Ionization of water in interfacial electric fields: An electrochemical view, *Chem. Phys. Lett.* **519-20**, 1 (2012).
[44]C. R. Song and P. S. Wang, High electric field effects on gigahertz dielectric properties of water measured with microwave microfluidic devices, *Rev. Sci. Instrum.* **81**, 054702 (2010).
[45]J. Dzubiella and J. P. Hansen, Electric-field-controlled water and ion permeation of a hydrophobic nanopore, *J. Chem. Phys.* **122**, 234706 (2005).
[46]J. Z. Wu, D. Bratko, and J. M. Prausnitz, Interaction between like-charged colloidal spheres in electrolyte solutions, *Proc. Natl. Acad. Sci.* **95**, 15169 (1998).
[47]D. Bratko, B. Jonsson, and H. Wennerstrom, Electrical double-layer interactions with image charges, *Chem. Phys. Lett.* **128**, 449 (1986).
[48]J. D. Smith, C. D. Cappa, K. R. Wilson, R. C. Cohen, P. L. Geissler, and R. J. Saykally, Unified description of temperature-dependent hydrogen-bond rearrangements in liquid water, *Proc. Natl. Acad. Sci.* **102**, 14171 (2005).
[49]B. Sellner, M. Valiev, and S. M. Kathmann, Charge and electric field fluctuations in aqueous NaCl electrolytes, *J. Phys. Chem. B* **117**, 10869 (2013).
[50]H. J. C. Berendsen, J. R. Grigera, and T. P. Straatsma, The missing term in effective pair potentials, *J. Phys. Chem.* **91**, 6269 (1987).
[51]G. Lamoureux, E. Harder, I. V. Vorobyov, B. Roux, and A. D. MacKerell, A polarizable model of water for molecular dynamics simulations of biomolecules, *Chem. Phys. Lett.* **418**, 245 (2006).

[52]P. T. Kiss and A. Baranyai, A systematic development of a polarizable potential of water, *J. Chem. Phys.* **138**, 204507 (2013).
[53]M. von Domaros, D. Bratko, B. Kirchner, and A. Luzar, Dynamics at a janus interface, *J. Phys. Chem. C* **117**, 4561 (2013).
[54]D. Bratko, C. D. Daub, and A. Luzar, Field-exposed water in a nanopore: Liquid or vapour?, *Phys. Chem. Chem. Phys.* **10**, 6807 (2008).
[55]J. R. Choudhuri, D. Vanzo, P. A. Madden, M. Salanne, D. Bratko, and A. Luzar, Dynamic response in nanoelectrowetting on a dielectric, *Acs Nano* **10**, 8536 (2016).
[56]C. D. Daub, N. M. Cann, D. Bratko, and A. Luzar, Electrokinetic flow of an aqueous electrolyte in amorphous silica nanotubes, *Phys. Chem. Chem. Phys.* **20**, 27838 (2018).
[57]M. Agarwal, M. P. Alam, and C. Chakravarty, Thermodynamic, diffusional, and structural anomalies in rigid-body water models, *J. Phys. Chem. B* **115**, 6935 (2011).
[58]P. Paricaud, M. Predota, A. A. Chialvo, and P. T. Cummings, From dimer to condensed phases at extreme conditions: Accurate predictions of the properties of water by a gaussian charge polarizable model, *J. Chem. Phys.* **122**, 244511 (2005).
[59]V. Ballenegger, Communication: On the origin of the surface term in the ewald formula, *J. Chem. Phys.* **140**, 161102 (2014).
[60]G. Bussi, D. Donadio, and M. Parrinello, Canonical sampling through velocity rescaling, *J. Chem. Phys.* **126**, 014101 (2007).
[61]S. Plimpton, Fast parallel algorithms for short-range molecular-dynamics, *J. Comput. Phys.* **117**, 1 (1995).
[62]B. Hess, C. Kutzner, D. van der Spoel, and E. Lindahl, Gromacs 4: Algorithms for highly efficient, load-balanced, and scalable molecular simulation, *J. Chem. Theory Comput.* **4**, 435 (2008).
[63]M. Sega, Bk3-water-model, https://github.Com/marcello-sega/gromacs.
[64]M. Brehm and B. Kirchner, Travis - a free analyzer and visualizer for monte carlo and molecular dynamics trajectories, *Journal of Chemical Information and Modeling* **51**, 2007 (2011).
[65]W. Humphrey, A. Dalke, and K. Schulten, Vmd: Visual molecular dynamics, *Journal of Molecular Graphics* **14**, 33 (1996).
[66]D. Laage and J. T. Hynes, On the molecular mechanism of water reorientation, *J. Phys. Chem. B* **112**, 14230 (2008).
[67]B. J. Berne, *Multiple Time Scales, eds. J. U. Brackbill and B. I. Cohen, Academic Press*, 419 (1985).
[68]D. Chandler, Statistical mechanics of isomerization dynamics in liquids and transition state approximation, *J. Chem. Phys.* **68**, 2959 (1978).
[69]A. Luzar and D. Chandler, Structure and hydrogen-bond dynamics of water-dimethyl sulfoxide mixtures by computer-simulations, *J. Chem. Phys.* **98**, 8160 (1993).
[70]D. Li and G. Z. Jia, Dielectric properties of spc/e and tip4p under the static electric field and microwave field, *Physica a-Statistical Mechanics and Its Applications* **449**, 348 (2016).
[71]S. J. Suresh, Disruption of hydrogen bond structure of water near charged electrode surfaces, *J. Chem. Phys.* **126** (2007).
[72]J. Y. Yan, S. D. Overduin, and G. N. Patey, Understanding electrofreezing in water simulations, *J. Chem. Phys.* **141**, 074501 (2014).
[73]F. Sedlmeier, D. Horinek, and R. R. Netz, Spatial correlations of density and structural fluctuations in liquid water: A comparative simulation study, *J. Am. Chem. Soc.* **133**, 1391 (2011).
[74]D. H. Jung, J. H. Yang, and M. S. Jhon, The effect of an external electric field on the structure of liquid water using molecular dynamics simulations, *Chem. Phys.* **244**, 331 (1999).

[75]R. D. Mountain and D. Thirumalai, Hydration for a series of hydrocarbons, *Proc. Natl. Acad. Sci.* **95**, 8436 (1998).
[76]J. R. Errington and P. G. Debenedetti, Relationship between structural order and the anomalies of liquid water, *Nature* **409**, 318 (2001).
[77]F. Rao, S. Garrett Roe, and P. Hamm, Structural inhomogeneity of water by complex network analysis, *J. Phys. Chem. B* **114**, 15598 (2010).
[78]I. M. Svishchev and P. G. Kusalik, Structure in liquid water - a study of spatial-distribution functions, *J. Chem. Phys.* **99**, 3049 (1993).
[79]S. V. Shevkunov and A. Vegiri, Equilibrium structures of the n = 64 water cluster in the presence of external electric fields, *J. Mol. Structure-Theochem* **574**, 27 (2001).
[80]I. M. Svishchev and P. G. Kusalik, Electrofreezing of liquid water: A microscopic perspective, *J. Am. Chem. Soc.* **118**, 649 (1996).
[81]C. D. Daub, K. Leung, and A. Luzar, Structure of aqueous solutions of monosodium glutamate, *J. Phys. Chem. B* **113**, 7687 (2009).
[82]A. Baranyai and P. T. Kiss, Polarizable model of water with field-dependent polarization, *J. Chem. Phys.* **135**, 234110 (2011).
[83]S. J. Suresh, A. V. Satish, and A. Choudhary, Influence of electric field on the hydrogen bond network of water, *J. Chem. Phys.* **124**, 074506 (2006).
[84]M. Girardi and W. Figueiredo, Three-dimensional square water in the presence of an external electric field, *J. Chem. Phys.* **125** (2006).
[85]E. Harder, J. D. Eaves, A. Tokmakoff, and B. J. Berne, Polarizable molecules in the vibrational spectroscopy of water, *Proc. Natl. Acad. Sci.* **102**, 11611 (2005).
[86]J. J. Loparo, S. T. Roberts, and A. Tokmakoff, Multidimensional infrared spectroscopy of water. Ii. Hydrogen bond switching dynamics, *J. Chem. Phys.* **125** (2006).
[87]N. Agmon, Liquid water: From symmetry distortions to diffusive motion, *Acc. Chem. Res.* **45**, 63 (2012).
[88]T. Kawasaki and K. Kim, Identifying time scales for violation/preservation of stokes-einstein relation in supercooled water, *Science Advances* **3** (2017).
[89]J. D. Eaves, A. Tokmakoff, and P. L. Geissler, Electric field fluctuations drive vibrational dephasing in water, *J. Phys. Chem. A* **109**, 9424 (2005).
[90]S. V. Shevkunov and A. Vegiri, Electric field induced transitions in water clusters, *J. Mol. Structure-Theochem* **593**, 19 (2002).

# Anisotropic Structure and Dynamics of Water under Static Electric Fields: Supplementary Material

Mahdi Shafiei[1], Michael von Domaros[2], Dusan Bratko[1], and Alenka Luzar[1]

[1]Department of Chemistry, Virginia Commonwealth University, Richmond, Virginia 23284-2006, United States.
[2] Department of Chemistry, University of California, Irvine, Irvine, California 92697, United States

## I. H-bond kinetic model

The Luzar/Chandler model describes the H-bond kinetics of hydrogen bond breaking and reforming between pairs of water molecules.[1] The model defines the state of hydrogen bonding by a dynamical variable $h(t)$, which is equal to 1 if a pair of molecules is H-bonded and zero otherwise. Given this variable, a H-bond time correlation function can be defined

$$c(t) = \frac{\langle h(t)h(0)\rangle}{\langle h\rangle}, \qquad \text{SM.1}$$

which is the probability that an initially ($t = 0$) hydrogen bonded pair of molecules is still bonded at time $t$, regardless of any breakings of H-bonds between these two times. The relaxation of an initial hydrogen bond populations towards equilibrium is given by

$$k(t) = -\frac{dc(t)}{dt} = \frac{\langle \dot{h}(0)h(t)\rangle}{\langle h\rangle}. \qquad \text{SM.2}$$

According to Luzar and Chandler, the decay of such populations can be understood phenomenologically by an equilibrium between states A and B,

$$\mathrm{A} \underset{k'}{\overset{k}{\rightleftharpoons}} \mathrm{B}, \qquad \text{SM.3}$$

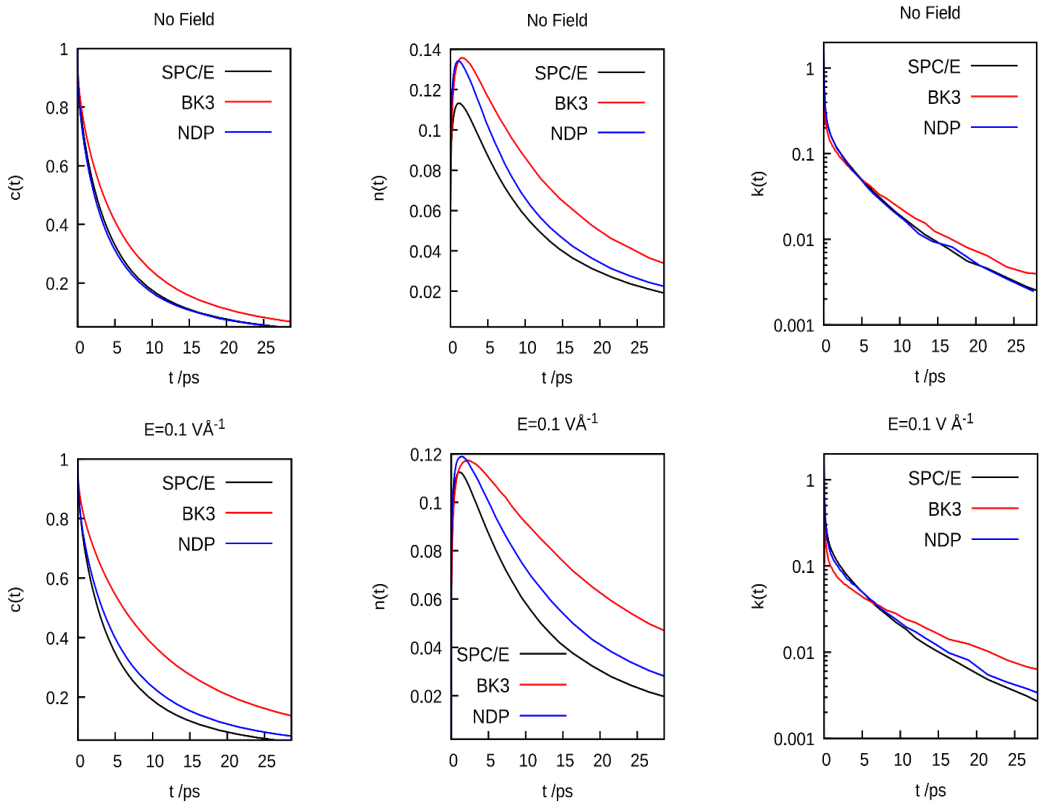


Figure S 1. The hydrogen bond time correlation functions (from left to right) c(t), n(t), and $k(t) = -dc/dt$ for various water models under zero field (top) and E = 0.1 $V\text{Å}^{-1}$ (bottom).

where A means a hydrogen bond between a tagged pair of water molecules exits ("ON") and B means the hydrogen bond has broken ("OFF"), but the pair has not yet diffused apart. The constants $k$ and $k'$ are the rates of H bond forming and breaking. Populations belonging to the state B are given by

$$n(t) = \frac{\langle h(0)[1 - h(t)]H(t)\rangle}{\langle h\rangle}, \qquad \text{SM.4}$$

where $H = 1$ if the pair has not diffused apart (the molecules are first shell neighbors).

Assuming first order kinetics, $-\frac{d[A]}{dt} = k[A] - k'[B]$, or expressed in terms of the respective time correlation functions,

$$k(t) = kc(t) - k'n(t), \qquad \text{SM.5}$$

we can find a pair of $k$ and $k'$ that best matches the simulation data.

In Figure S 1 we show the time correlation functions $c(t)$, $n(t)$, and $k(t)$ for the original model and for all three water models under zero E-field and under $E = 0.1\ V\text{Å}^{-1}$. In Figure S 2, we show the corresponding correlation plots used for calculating the pair of rate constants according to eq. SM. 5.

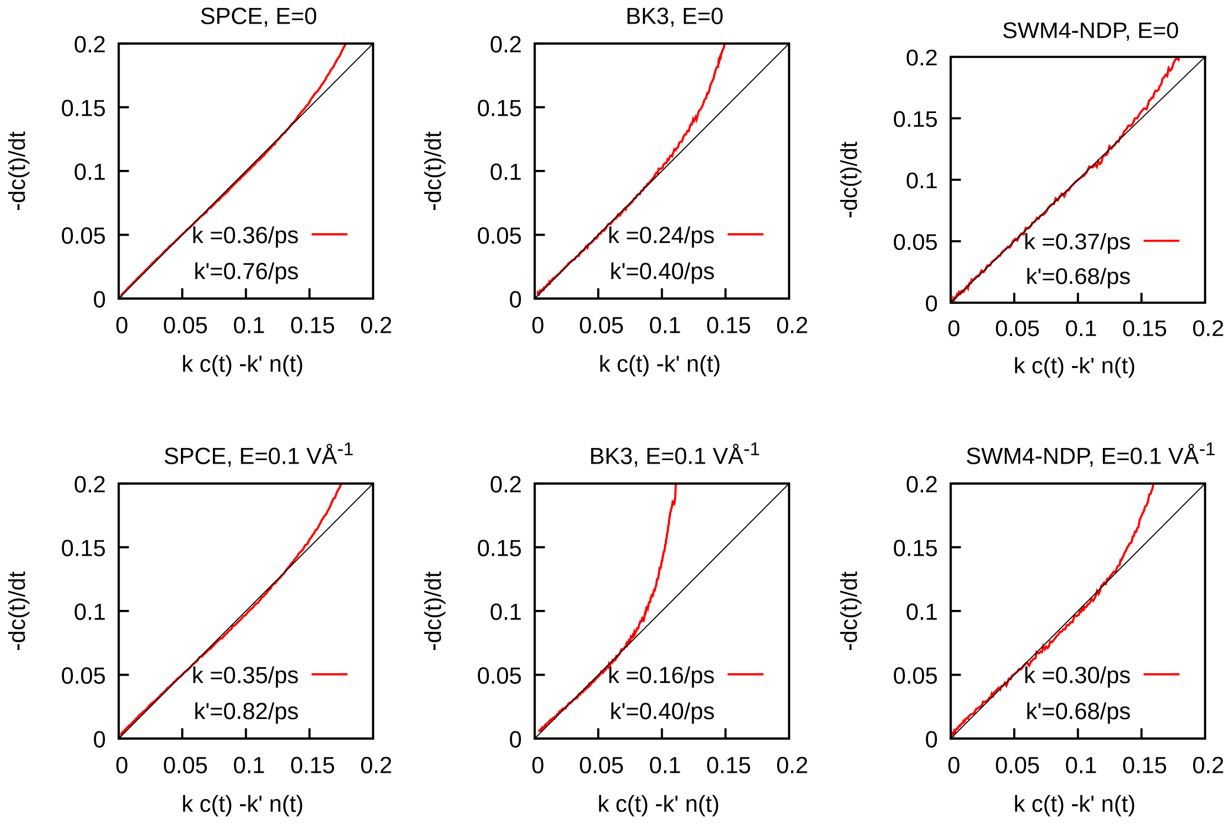


Figure S 2. Hydrogen bond kinetics correlation plots. For classic model, red lines, showing the best fit between $k(t)$ (y-axis) and $k\ c(t) - k'n(t)$ to find the rate constantst $k$ and $k'$in SPC/E (left), BK3 (middle) and SWM4-NDP (right) for zero field (top) and E $= 0.1\ V\text{Å}^{-1}$ (bottom).

## II. The relation between diffusion coefficient and the hydrogen bond dynamics

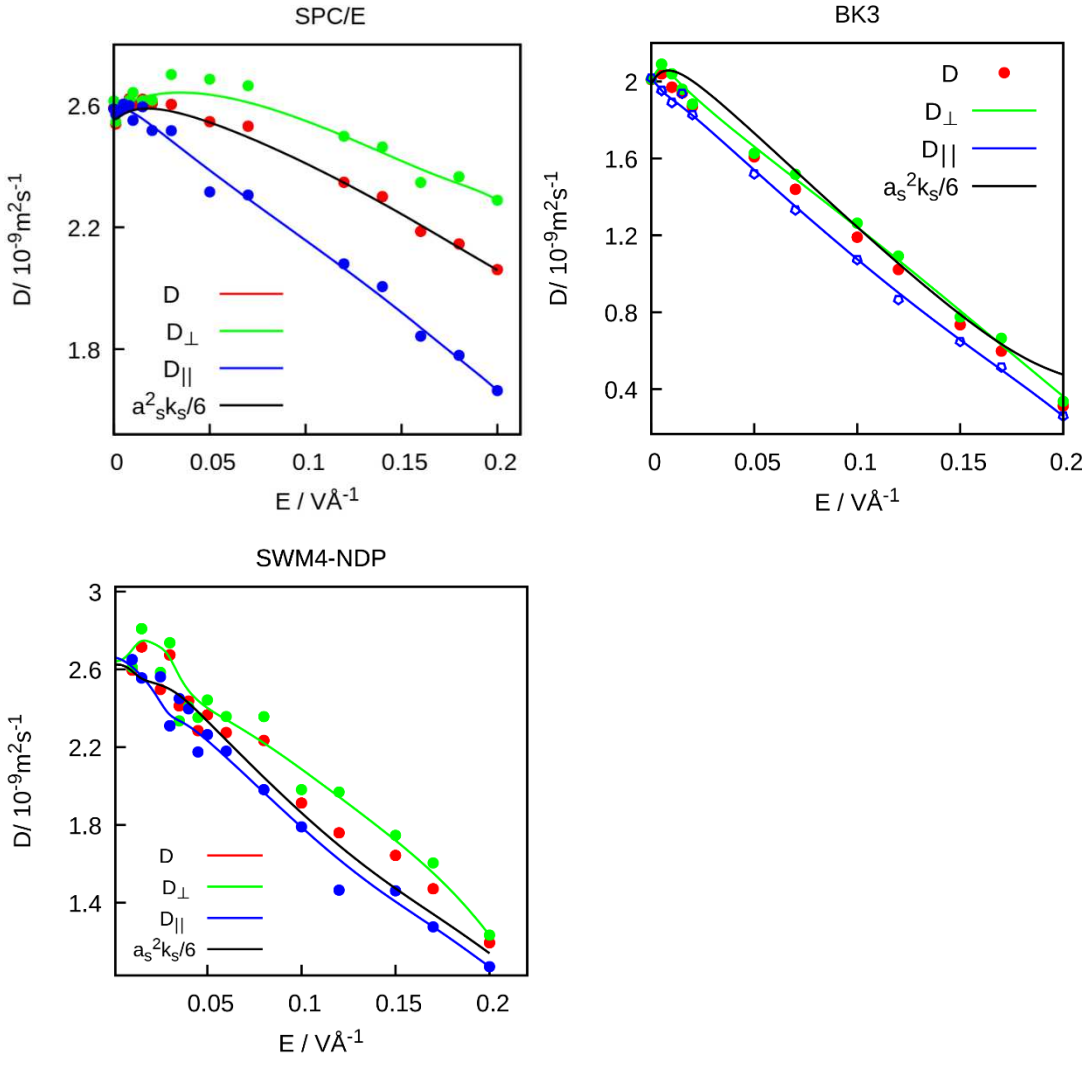


Figure S 3. Isotropic diffusion coefficients $D$ as well as the parallel, $D_{\parallel}$ , and perpendicular components $D_{\perp}$ of the diffusion tensor in SPC/E water (top left), BK3 water (top right), and SWM4-NDP water(bottom). The black line is the best fit of the overall diffusion coefficient to a random walk characterized by the frequency of H-bond switching. Green and blue lines are included as a guide to the eye.

## III. Tetrahedral order parameter

We calculated the tetrahedral order parameter[2]

$$q = 1 - \frac{3}{8}\sum_{j=1}^{3}\sum_{k=j+1}^{4}\left(cos\psi_{jk} + \frac{1}{3}\right)^2. \qquad \text{SM.6}$$

and results for all water models subject to E-fields between 0 and 0.2 $V\text{Å}^{-1}$ are shown in Table S. 1. An increase in $q$ is required but not sufficient to prove an increase in tetrahedrality.[3] These results show that the tetrahedral structure of SPC/E[4] water does not change under static E-fields, whereas the order parameters of BK3[5] and SWM4-NDP[6] water change by around 8% and 10%, respectively, under the strongest investigated electric fields.

Table S. 1. Order parameters q for different static E-fields.

| E-fields | $q$ | | |
|---|---|---|---|
| | SPC/E | BK3 | SWM4-NDP |
| $E = 0$ | 0.64 | 0.67 | 0.62 |
| $E = 0.05\ V\text{Å}^{-1}$ | 0.64 | 0.67 | 0.63 |
| $E = 0.1\ V\text{Å}^{-1}$ | 0.64 | 0.69 | 0.64 |
| $E = 0.2\ V\text{Å}^{-1}$ | 0.65 | 0.74 | 0.67 |

## IV. Oxygen hydrogen and hydrogen-hydrogen radial distribution function

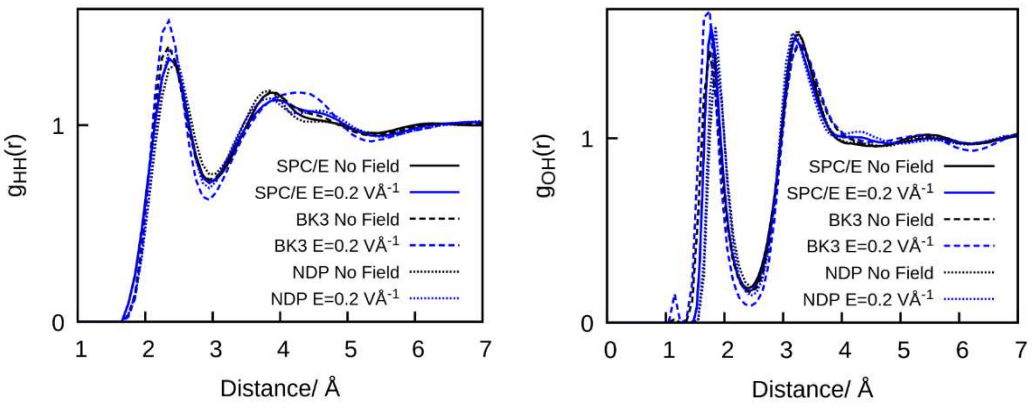


Figure S 4. The hydrogen-hydrogen and oxygen-hydrogen radial distribution functions $g_{HH}(r)$ and $g_{OH}(r)$ for zero E-field and $E = 0.2\ V\text{Å}^{-1}$.

## V. Directional distribution function for BK3 and SWM4-NDP

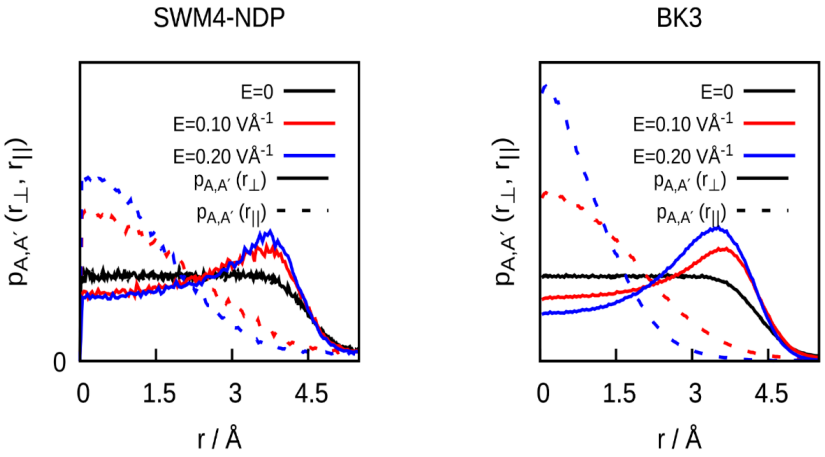


Figure S 5. Anisotropic radial distribution functions between two acceptor molecules A and A′ joined by a common donor, $p_{AA'}(r_{\parallel})$ and $p_{AA'}(r_{\perp})$, for BK3 and SWM4-NDP water models.

## VI. Spatial distribution functions

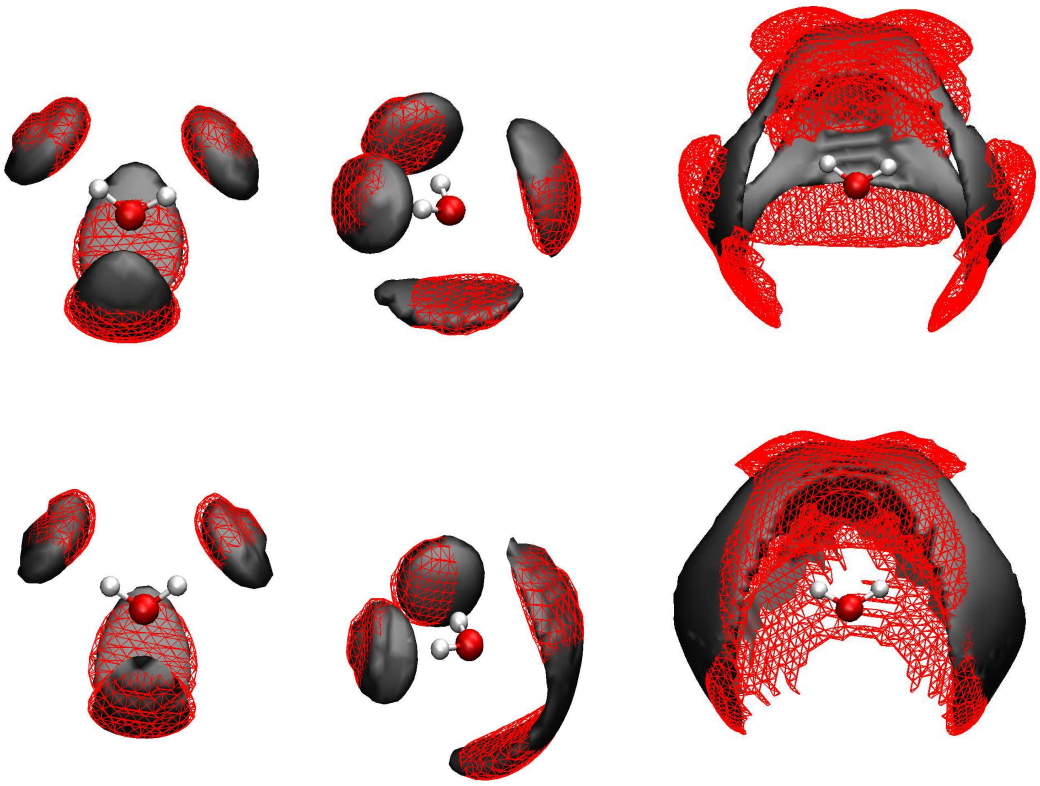

Figure S 6. The spatial distribution functions[7] of BK3 water (top) and SWM4-NDP (bottom) water in the first (left and center) and the second (right) coordination shell for no field (black) and $\mathrm{E} = 0.2\ \mathrm{V\AA^{-1}}$ (red). The corresponding iso-densities are 1.8 and 1.3, respectively. The central molecules have been added to show the reference coordinate system.

### References


1 A. Luzar and D. Chandler, "Hydrogen-bond kinetics in liquid water," Nature **379**, 55 (1996).

2 J. R. Errington and P. G. Debenedetti, "Relationship between structural order and the anomalies of liquid water," Nature **409**, 318 (2001).

3 E. Duboue, D. Laage, E. Normale, E. Duboué-Dijon and D. Laage, "Characterization of the Local Structure in Liquid Water by Various Order Parameters," J. Phys. Chem. B **119**, 8406 (2015).

4 H. J. C. Berendsen, J. R. Grigera and T. P. Straatsma, "The Missing Term in Effective Pair Potentials," J. Phys. Chem. **91**, 6269 (1987).

5 P. T. Kiss and A. Baranyai, "A systematic development of a polarizable potential of water,"

J. Chem. Phys. **138**, 204507 (2013).

6 G. Lamoureux, E. Harder, I. V. Vorobyov, B. Roux and A. D. MacKerell, "A polarizable model of water for molecular dynamics simulations of biomolecules," Chem. Phys. Lett. **418**, 245 (2006).

7 I. M. Svishchev and P. G. Kusalik, "Structure in liquid water: A study of spatial distribution functions," J. Chem. Phys. **99**, 3049 (1993).